UCSF

UC San Francisco Electronic Theses and Dissertations

Title

Disease-Associated Mutations in Human BICD2 Hyperactivate Motility of Dynein-Dynactin

Permalink

https://escholarship.org/uc/item/9p33d5tj

Author

Huynh, Walter

Publication Date

2017

Supplemental Material

https://escholarship.org/uc/item/9p33d5tj#supplemental

Peer reviewed|Thesis/dissertation

Disease-Associated Mutations In Human BICD2 Hyperactivate
Motility Of Dynein-Dynactin

by

Walter Q. Huynh

DISSERTATION

Submitted in partial satisfaction of the requirements for the degree of

DOCTOR OF PHILOSOPHY

in

Biochemistry and Molecular Biology

in the

Dedicated to my family.

Acknowledgements

The Vale lab is a wonderful place. The collection of people that Ron has assembled are fantastic on both a personal and scientific level. Special thanks in particular to Richard McKenney, who took on the role of post-doc mentor with no complaint and taught me a lot of invaluable lessons, both science and otherwise. The three structural pillars of the lab: Phoebe Grigg, Nan Zhang, and Nico Stuurman were also all essential in their own ways. Rather than list out all the names of other past and present lab members, as you have all been truly helpful in this journey, I'd like to just give a blanket thank you to everyone else. You people rock.

I've learned a lot from watching how Ron operates the lab. Seeing firsthand how he tackles big problems, whether it's reforming the publishing system or figuring out how to better communicate science to the public, will never cease to amaze me. Even through all this, he finds time to be a great mentor. Thanks Ron, for all your help. You've been inspirational.

I'd also like to thank my thesis committee consisting of David Agard and Jeremy Reiter for their advice and discussion regarding my project and general life plans. Thanks to my friends, both new and old, for providing a distraction from lab when needed.

My greatest thanks go out to my family, who have provided motivation, support, and everything else that was required to finish this work. My parents have strived to ensure that my sister and I can have the opportunity to pursue our dreams and goals, sacrificing theirs in the process. My sister and my brother-in-law constantly looked out for me and always made sure that I always had enough food to eat. Lastly, thanks to my mutts Obee, Dory, and Emily for keeping me sane and giving me much needed exercise in the form of walks.

Investigation of BICD2 Disease-Associated Mutations

By Walter Huynh

Mammalian cytoplasmic dynein is a microtubule-based motor that is involved in many cellular functions, one of which includes the retrograde transport of cargo. In contrast to yeast dynein, which is processive on its own, mammalian dynein requires both an adaptor protein and dynactin in order to achieve micron long run-lengths. Bicaudal D2 (BICD2), a protein comprised of three distinct coiled-coils, is one such adaptor. Recent studies have reported that mutations in BICD2 are associated with neurodegenerative diseases that include spinal muscular atrophy. In this dissertation, I demonstrate through biochemical and single molecule microscopy assays that full-length BICD2 is auto-inhibited and can be activated to interact with dynein and dynactin via the addition of one of its interacting partners, Rab6a. Testing of four BICD2 disease-associated mutations with this same set of assays reveal that, compared to wild-type, the mutants exhibit an increased formation of motile motor complexes. I further confirm this finding by developing an in vitro cargo reconstitution assay using liposomes as proxies for vesicles. This apparent ability to increase transport by the mutants is also observed in cells using an inducible re-localization system with peroxisomes. When overexpressed in rat hippocampal neurons, the BICD2 mutants lead to decreased neurite growth. Altogether, this work shows that dominant mutations in BICD2 hyperactivate dynein-driven motility

and suggest that an imbalance of minus versus plus end–directed microtubule motility

in neurons may underlie spinal muscular atrophy.

Table of Contents

Chapter 1

Chapter 2

Chapter 3

Appendix A

List of Figures

Chapter I

Introduction

Introduction

The eukaryotic cell is a complex landscape of activities. One critical element in this bustling environment is the ability to transport things from one cellular location to another in cases where simple diffusion is not sufficient. This directed transport is mediated by molecular motors that hydrolyze ATP in order to take steps along a cytoskeletal track comprised of either microtubules or actin. There exist two types of motors that translocate on polarized microtubule filaments: kinesin and dynein. Most kinesins migrate towards the plus-end of the microtubules, while the bulk of the minus-end activity is performed by the megadalton protein complex, dynein (Allan, 2011).

Cytoplasmic dynein was originally identified as a microtubule-associated protein in 1987 that possessed ATPase activity (Paschal et al., 1987). Since then, work from many different labs have contributed to a core understanding of the roles and means in which it participates in cellular functions. Included in this is how cytoplasmic dynein transports cargo that include vesicles, organelles, and viruses; its role in nuclear positioning; and its function in mitotic chromosome alignment (Allan, 2011). The ability to purify recombinant yeast dynein subsequently accelerated the acquisition of structural and biochemical knowledge of the protein (Reck-Peterson et al., 2006; Carter et al., 2011).

More recently, it was shown that mammalian dynein is dissimilar from its yeast homolog in that it requires additional binding partners in order to move stably along a

microtubule (McKenney et al., 2014; Schlager et al., 2014a). These two factors, dynactin and an adaptor protein, facilitate the formation of a processive tripartite complex. In their absence, mammalian dynein can bind and diffuse along microtubules, but is unable to undertake the long run lengths that are observed in cells. The initial adaptor protein identified, Bicaudal D2 (BICD2), had previously been shown to be associated with dynein, but its role in stabilizing this ternary complex formation was new and unexpected (Splinter et al., 2012a).

The native cargo for BICD2 includes the small GTPase Rab6 and RanBP2, each of which have very specific roles and locales in which they function. A problem arises then that while BICD2 might be a very capable adaptor protein, it is restricted in that it can only conjugate dynein and dynactin to its relatively limited set of interaction partners. It was thus feasible that there might be other adaptor proteins that would recruit and mediate specific transport to other cellular locations in order to circumvent this limitation. Part of the early work of my doctoral work involved working with Richard McKenney to determine whether this hypothesis was true. Through examination of the literature and selectively purifying proteins that had known associations with dynein, we were able to identify additional adaptor proteins, including Rab11-FIP3, the mitotic protein Spindly, and Hook3 (McKenney et al., 2014). These proteins, when added to purified dynein and dynactin, were sufficient to elicit the same robust motility that BICD2 conferred. This is by no means an exhaustive list of adaptors; indeed, a group recently

identified two additional adaptors, ninein and ninein-like protein, by utilizing the Bio-ID system in conjunction with IP-MS (Redwine and Reck-Peterson, 2017).

A better understanding of dynein and its associated factors is informative from both a basic science perspective as well as a clinical one. As mentioned, dynein performs multiple roles in a cell. Given the importance of retrograde cargo transport alone, particularly in cell types like neurons that contain processes up to one meter, it is not too surprising that mutations in dynein that alter motor function have been implicated in a wide range of neurodegenerative and neurodevelopmental diseases. Initial studies showed that two mutagenized mice strains, *Cra1* and *Loa*, exhibited locomotor disorders that were attributed to mutations in the gene encoding dynein heavy chain (Hafezparast et al., 2003). It was later shown that *Loa* mice are defective in retrograde axonal transport; this phenotype is probably caused by both the fact that the mutated motor has a markedly reduced run length and that it has a lower binding affinity to dynactin and other associated partners (Ori-McKenney et al., 2010; Deng et al., 2010). To date, dynein impairment is complicit in diseases that include spinal muscular atrophy, amyotrophic lateral sclerosis, Charcot-Marie-Tooth disease, Alzheimer's disease, Parkinson's disease, and Huntington's disease (Chen et al., 2014).

The discovery that adaptors are required for mammalian dynein function opened up the possibility that defects in these proteins might also contribute to similar types of disorders. Indeed, genome-wide studies examining patients afflicted with spinal

muscular atrophy, lower extremity dominant (SMA-LED) identified the *BICD2* locus as a hotbed for mutations (Martinez-Carrera and Wirth, 2015; Peeters et al., 2013; Neveling et al., 2013). The most common form of spinal muscular atrophy is recessive and is usually caused by mutations or deletions in the gene encoding the survival of motor neurons (SMN1). This eventually results in degeneration of the anterior horn cells and leads to muscle atrophy and weakness (Rossor et al., 2014). Patients afflicted with the genetically dominant form of SMA caused by mutations in BICD2 also exhibit similar clinical symptoms of muscle weakness and wasting, primarily in the lower limbs. Functional characterization of select mutants showed that some of them bound to the dynein intermediate chain with a higher affinity than wildtype (Oates et al., 2013). The effect that this has on the adaptor is unclear; over-expression of some of these same mutants in cell results in Golgi fragmentation, a phenotype commonly associated with the inhibition of dynein function (Neveling et al., 2013).

In order to further understand how these mutations might be contributing to the disease etiology, I utilized both biochemical and cellular assays to identify the functional changes that these changes rendered in the adaptor. The in vitro assays that are utilized to analyze single molecule dynein movement were ideal for examining how these single amino acid changes in BICD2 disrupted its normal behavior. Parameters including run length, velocity, and frequency of motile events are all measurable with purified motor complexes. Using these assays, I first verified that full-length BICD2 could be activated

by Rab6a bound to GTP, but not GDP. I then found that the BICD2 mutants tested all exhibited an increased in their ability to recruit dynein and dynactin and form motile complexes. This could be either due to the point mutations enhancing the affinity to dynein and dynactin, or alternatively, the mutations destabilized the inhibitory confirmation and made BICD2 more readily active. Assays using an N-terminal construct lacking the inhibitory C-terminal domain indicate that the latter seems to be the case.

Using a cell-based recruitment assay, I was then able to demonstrate that this behavior is present in the more complex environment of the cytoplasm as well. Intriguingly, while overexpression of wild-type BICD2 in E18 rat hippocampal neurons resulted in no observable changes in total neurite length, the BICD2 mutants caused a roughly 40% decrease. Altogether, my doctoral work provides insight into how mutations in a dynein adaptor can result in hyperactivation of retrograde motility. While the exact mechanism in which this causes diseases like spinal muscular atrophy is still unclear, it suggests that increasing minus-end transport, causing either an imbalance in cargo localization or changing the distribution of dynein, is a contributing factor.

References

Aitken, C.E., R.A. Marshall, and J.D. Puglisi. 2008. An oxygen scavenging system for improvement of dye stability in single-molecule fluorescence experiments. *Biophys. J.* 94:1826–1835. doi:10.1529/biophysj.107.117689.

Allan, V.J. 2011. Cytoplasmic dynein. *Biochem. Soc. Trans.* 39:1169–78. doi:10.1042/BST0391169.

Burkhardt, J.K., C.J. Echeverri, T. Nilsson, and R.B. Vallee. 1997. Overexpression of the dynamitin (p50) subunit of the dynactin complex disrupts dynein-dependent maintenance of membrane organelle distribution. *J. Cell Biol.* 139:469–484. doi:10.1083/jcb.139.2.469.

Carter, A.P., C. Cho, L. Jin, and R.D. Vale. 2011. Crystal structure of the dynein motor domain. *Science*. 331:1159–65. doi:10.1126/science.1202393.

de Chaumont, F., S. Dallongeville, N. Chenouard, N. Hervé, S. Pop, T. Provoost, V. Meas-Yedid, P. Pankajakshan, T. Lecomte, Y. Le Montagner, T. Lagache, A. Dufour, and J.-C. Olivo-Marin. 2012. Icy: an open bioimage informatics platform for extended reproducible research. *Nat. Methods*. 9:690–696. doi:10.1038/nmeth.2075.

Chen, X.J., H. Xu, H.M. Cooper, and Y. Liu. 2014. Cytoplasmic dynein: A key player in neurodegenerative and neurodevelopmental diseases. *Sci. China Life Sci.* 57:372–377. doi:10.1007/s11427-014-4639-9.

Cianfrocco, M.A., M.E. Desantis, A.E. Leschziner, and S.L. Reck-peterson. 2015. Mechanism and Regulation of Cytoplasmic Dynein. 1–26. doi:10.1146/annurev-cellbio-100814-125438.

Deng, W., C. Garrett, B. Dombert, V. Soura, G. Banks, E.M.C. Fisher, M.P. Van Der Brug, and M. Hafezparast. 2010. Neurodegenerative mutation in cytoplasmic dynein alters its organization and dynein-dynactin and dynein-kinesin interactions. *J. Biol. Chem.* 285:39922–39934. doi:10.1074/jbc.M110.178087.

Dimitriadi, M., A. Derdowski, G. Kalloo, M.S. Maginnis, B. Bliska, A. Sorkaç, K.C. Q Nguyen, S.J. Cook, G. Poulogiannis, W.J. Atwood, D.H. Hall, A.C. Hart, and E.H. by Robert Horvitz. 2016. Decreased function of survival motor neuron protein impairs endocytic pathways. doi:10.1073/pnas.1600015113.

Edelstein, A., N. Amodaj, K. Hoover, R. Vale, and N. Stuurman. 2010. Computer control of microscopes using manager. *Curr. Protoc. Mol. Biol.* 1–17. doi:10.1002/0471142727.mb1420s92.

Gama, J.B., C. Pereira, P.A. Simões, R. Celestino, R.M. Reis, D.J. Barbosa, H.R. Pires, C.

Carvalho, J. Amorim, A.X. Carvalho, D.K. Cheerambathur, and R. Gassmann. 2017. Molecular mechanism of dynein recruitment to kinetochores by the Rod–Zw10–Zwilch complex and Spindly. *J. Cell Biol.* 216:943–960. doi:10.1083/jcb.201610108.

Grigoriev, I., D. Splinter, N. Keijzer, P.S. Wulf, J. Demmers, T. Ohtsuka, M. Modesti, I. V Maly, F. Grosveld, C.C. Hoogenraad, and A. Akhmanova. 2007. Rab6 regulates transport and targeting of exocytotic carriers. *Dev. Cell*. 13:305–14. doi:10.1016/j.devcel.2007.06.010.

Hafezparast, M., R. Klocke, C. Ruhrberg, A. Marquardt, A. Ahmad-Annuar, S. Bowen, G. Lalli, A.S. Witherden, H. Hummerich, S. Nicholson, P.J. Morgan, R. Oozageer, J. V Priestley, S. Averill, V.R. King, S. Ball, J. Peters, T. Toda, A. Yamamoto, Y. Hiraoka, M. Augustin, D. Korthaus, S. Wattler, P. Wabnitz, C. Dickneite, S. Lampel, F. Boehme, G. Peraus, A. Popp, M. Rudelius, J. Schlegel, H. Fuchs, M. Hrabe de Angelis, G. Schiavo, D.T. Shima, A.P. Russ, G. Stumm, J.E. Martin, and E.M.C. Fisher. 2003. Mutations in dynein link motor neuron degeneration to defects in retrograde transport. *Science*. 300:808–12. doi:10.1126/science.1083129.

Harada, A., Y. Takei, Y. Kanai, Y. Tanaka, S. Nonaka, and N. Hirokawa. 1998. Golgi vesiculation and lysosome dispersion in cells lacking cytoplasmic dynein. *J. Cell Biol.* 141:51–59. doi:10.1083/jcb.141.1.51.

Hoang, H.T., M.A. Schlager, A.P. Carter, and S.L. Bullock. 2017. DYNC1H1 mutations associated with neurological diseases compromise processivity of dynein-dynactin-cargo adaptor complexes. *Proc. Natl. Acad. Sci.* 114:1–19. doi:10.1073/pnas.1620141114.

Hoogenraad, C.C., P. Wulf, N. Schiefermeier, T. Stepanova, N. Galjart, J.V. Small, F. Grosveld, C.I. de Zeeuw, and A. Akhmanova. 2003. Bicaudal D induces selective dynein-mediated microtubule minus end-directed transport. *EMBO J.* 22:6004–15. doi:10.1093/emboj/cdg592.

Jaarsma, D., R. van den Berg, P.S. Wulf, S. van Erp, N. Keijzer, M. a Schlager, E. de Graaff, C.I. De Zeeuw, R.J. Pasterkamp, A. Akhmanova, and C.C. Hoogenraad. 2014. A role for Bicaudal-D2 in radial cerebellar granule cell migration. *Nat. Commun.* 5:3411. doi:10.1038/ncomms4411.

Kapitein, L.C., M.A. Schlager, W.A. Van Der Zwan, P.S. Wulf, N. Keijzer, and C.C. Hoogenraad. 2010. Probing intracellular motor protein activity using an inducible cargo trafficking assay. *Biophys. J.* 99:2143–2152. doi:10.1016/j.bpj.2010.07.055.

Liu, Y., H.K. Salter, A.N. Holding, C.M. Johnson, E. Stephens, P.J. Lukavsky, J. Walshaw, and S.L. Bullock. 2013. Bicaudal-D uses a parallel, homodimeric coiled coil with heterotypic registry to coordinate recruitment of cargos to dynein. *Genes*

Dev. 27:1233–46. doi:10.1101/gad.212381.112.

Martinez-Carrera, L.A., and B. Wirth. 2015. Dominant spinal muscular atrophy is caused by mutations in BICD2, an important golgin protein. *Front. Neurosci.* 9. doi:10.3389/fnins.2015.00401.

Matanis, T., A. Akhmanova, P. Wulf, E. Del Nery, T. Weide, T. Stepanova, N. Galjart, F. Grosveld, B. Goud, C.I. De Zeeuw, A. Barnekow, and C.C. Hoogenraad. 2002. Bicaudal-D regulates COPI-independent Golgi-ER transport by recruiting the dynein-dynactin motor complex. *Nat. Cell Biol.* 4:986–92. doi:10.1038/ncb891.

McKenney, R.J., W. Huynh, M.E. Tanenbaum, G. Bhabha, and R.D. Vale. 2014. Activation of cytoplasmic dynein motility by dynactin-cargo adapter complexes. *Science (80-.).* 345:337–341. doi:10.1126/science.1254198.

Mohler, J., and E.F. Wieschaus. 1986. Dominant maternal-effect mutations of Drosophila melanogaster causing the production of double-abdomen embryos. *Genetics.* 112:803–822.

Mounier, J., G. Boncompain, L. Senerovic, T. Lagache, F. Chrétien, F. Perez, M. Kolbe, J.C. Olivo-Marin, P.J. Sansonetti, and N. Sauvonnet. 2012. Shigella effector IpaB-induced cholesterol relocation disrupts the golgi complex and recycling network to inhibit host cell secretion. *Cell Host Microbe.* 12:381–389. doi:10.1016/j.chom.2012.07.010.

Neveling, K., L. a Martinez-Carrera, I. Hölker, A. Heister, A. Verrips, S.M. Hosseini-Barkooie, C. Gilissen, S. Vermeer, M. Pennings, R. Meijer, M. te Riele, C.J.M. Frijns, O. Suchowersky, L. MacLaren, S. Rudnik-Schöneborn, R.J. Sinke, K. Zerres, R.B. Lowry, H.H. Lemmink, L. Garbes, J. a Veltman, H.J. Schelhaas, H. Scheffer, and B. Wirth. 2013. Mutations in BICD2, which encodes a golgin and important motor adaptor, cause congenital autosomal-dominant spinal muscular atrophy. *Am. J. Hum. Genet.* 92:946–54. doi:10.1016/j.ajhg.2013.04.011.

Oates, E.C., A.M. Rossor, M. Hafezparast, M. Gonzalez, F. Speziani, D.G. MacArthur, M. Lek, E. Cottenie, M. Scoto, a R. Foley, M. Hurles, H. Houlden, L. Greensmith, M. Auer-Grumbach, T.R. Pieber, T.M. Strom, R. Schule, D.N. Herrmann, J.E. Sowden, G. Acsadi, M.P. Menezes, N.F. Clarke, S. Züchner, F. Muntoni, K.N. North, and M.M. Reilly. 2013. Mutations in BICD2 cause dominant congenital spinal muscular atrophy and hereditary spastic paraplegia. *Am. J. Hum. Genet.* 92:965–73. doi:10.1016/j.ajhg.2013.04.018.

Ori-McKenney, K.M., J. Xu, S.P. Gross, and R.B. Vallee. 2010. A cytoplasmic dynein tail mutation impairs motor processivity. *Nat. Cell Biol.* 12:1228–1234. doi:10.1038/ncb2127.

Paschal, B.M., H.S. Shpetner, and R.B. Vallee. 1987. MAP 1C is a microtubule-activated ATPase which translocates microtubules in vitro and has dynein-like properties. *J. Cell Biol.* 105:1273–1282. doi:10.1083/jcb.105.3.1273.

Peeters, K., S. Bervoets, T. Chamova, I. Litvinenko, E. De Vriendt, S. Bichev, D. Kancheva, V. Mitev, M. Kennerson, V. Timmerman, P. De Jonghe, I. Tournev, J. Macmillan, and A. Jordanova. 2015. Novel mutations in the DYNC1H1 tail domain refine the genetic and clinical spectrum of dyneinopathies. *Hum. Mutat.* 36:287–291. doi:10.1002/humu.22744.

Peeters, K., I. Litvinenko, B. Asselbergh, L. Almeida-Souza, T. Chamova, T. Geuens, E. Ydens, M. Zimoń, J. Irobi, E. De Vriendt, V. De Winter, T. Ooms, V. Timmerman, I. Tournev, and A. Jordanova. 2013. Molecular Defects in the Motor Adaptor BICD2 Cause Proximal Spinal Muscular Atrophy with Autosomal-Dominant Inheritance. *Am. J. Hum. Genet.* 92:955–964. doi:10.1016/j.ajhg.2013.04.013.

Reck-Peterson, S.L., A. Yildiz, A.P. Carter, A. Gennerich, N. Zhang, and R.D. Vale. 2006. Single-Molecule Analysis of Dynein Processivity and Stepping Behavior. *Cell*. 126:335–348. doi:10.1016/j.cell.2006.05.046.

Redwine, W.B., and S.L. Reck-Peterson. 2017. The Human Cytoplasmic Dynein INteractome Reveals Novel Activators of Motility. *Elife*.

Rossor, A.M., E.C. Oates, H.K. Salter, Y. Liu, S.M. Murphy, R. Schule, M. a Gonzalez, M. Scoto, R. Phadke, C. a Sewry, H. Houlden, A. Jordanova, I. Tournev, T. Chamova, I. Litvinenko, S. Zuchner, D.N. Herrmann, J. Blake, J.E. Sowden, G. Acsadi, M.L. Rodriguez, M.P. Menezes, N.F. Clarke, M. Auer Grumbach, S.L. Bullock, F. Muntoni, M.M. Reilly, and K.N. North. 2014. Phenotypic and molecular insights into spinal muscular atrophy due to mutations in BICD2. *Brain*. doi:10.1093/brain/awu356.

Schlager, M.A., H.T. Hoang, L. Urnavicius, S.L. Bullock, and A.P. Carter. 2014a. In vitro reconstitution of a highly processive recombinant human dynein complex. *EMBO J.* 33:1855–68. doi:10.15252/embj.201488792.

Schlager, M.A., H.T. Hoang, L. Urnavicius, S.L. Bullock, and A.P. Carter. 2014b. In vitro reconstitution of a highly processive recombinant human dynein complex. *EMBO J.* 33:1855–68. doi:10.15252/embj.201488792.

Schlager, M.A., A. Serra-Marques, I. Grigoriev, L.F. Gumy, M. Esteves da Silva, P.S. Wulf, A. Akhmanova, and C.C. Hoogenraad. 2014c. Bicaudal D Family Adaptor Proteins Control the Velocity of Dynein-Based Movements. *Cell Rep.* 1–9. doi:10.1016/j.celrep.2014.07.052.

Schlager, M. a, L.C. Kapitein, I. Grigoriev, G.M. Burzynski, P.S. Wulf, N. Keijzer, E. de Graaff, M. Fukuda, I.T. Shepherd, A. Akhmanova, and C.C. Hoogenraad. 2010. Pericentrosomal targeting of Rab6 secretory vesicles by Bicaudal-D-related protein 1 (BICDR-1) regulates neuritogenesis. *EMBO J.* 29:1637–51. doi:10.1038/emboj.2010.51.

Schroeder, C.M., and R.D. Vale. 2016. Assembly and activation of dynein-dynactin by the cargo adaptor protein Hook3. *J. Cell Biol.* 214:309–318. doi:10.1083/jcb.201604002.

Splinter, D., D.S. Razafsky, M. a Schlager, A. Serra-Marques, I. Grigoriev, J. Demmers, N. Keijzer, K. Jiang, I. Poser, A. a Hyman, C.C. Hoogenraad, S.J. King, and A. Akhmanova. 2012a. BICD2, dynactin, and LIS1 cooperate in regulating dynein recruitment to cellular structures. *Mol. Biol. Cell*. 23:4226–41. doi:10.1091/mbc.E12-03-0210.

Splinter, D., D.S. Razafsky, M. a Schlager, A. Serra-Marques, I. Grigoriev, J. Demmers, N. Keijzer, K. Jiang, I. Poser, A. a Hyman, C.C. Hoogenraad, S.J. King, and A. Akhmanova. 2012b. BICD2, dynactin, and LIS1 cooperate in regulating dynein recruitment to cellular structures. *Mol. Biol. Cell*. 23:4226–41. doi:10.1091/mbc.E12-03-0210.

Teuling, E., V. van Dis, P.S. Wulf, E.D. Haasdijk, A. Akhmanova, C.C. Hoogenraad, and D. Jaarsma. 2008. A novel mouse model with impaired dynein/dynactin function develops amyotrophic lateral sclerosis (ALS)-like features in motor neurons and improves lifespan in SOD1-ALS mice. *Hum. Mol. Genet.* 17:2849–2862. doi:10.1093/hmg/ddn182.

Thorn, K.S., J.A. Ubersax, and R.D. Vale. 2000. Engineering the processive run length of the kinesin motor. *J. Cell Biol.* 151:1093–1100. doi:10.1083/jcb.151.5.1093.

Unger, A., G. Dekomien, A. Güttsches, R. Kley, M. Tegenthoff, A. Ferbert, J. Weis, W.A. Linke, L. Martinez-carrera, and M. Storbeck. 2016. Expanding the phenotype of BICD2 mutations toward skeletal muscle involvement. 1–10.

Utskarpen, A., H.H. Slagsvold, T.-G. Iversen, S. Walchli, and K. Sandvig. 2006. Transport of ricin from endosomes to the golgi apparatus is regulated by Rab6A and Rab6A??? *Traffic*. 7:663–672. doi:10.1111/j.1600-0854.2006.00418.x.

Wharton, R.P., and G. Struhl. 1989. Structure of the Drosophila BicaudalD protein and its role in localizing the posterior determinant nanos. *Cell*. 59:881–892. doi:10.1016/0092-8674(89)90611-9.

Chapter II

Investigation of BICD2 Disease-Associated Mutations

Disease-associated mutations in human BICD2 hyperactivate motility of dynein–dynactin

Walter Huynh[1,2], Ron Vale[1,2]

[1]The Howard Hughes Medical Institute, University of California, San Francisco, San Francisco, California, USA.

[2]Department of Cellular and Molecular Pharmacology, University of California, San Francisco, San Francisco, California, USA.

Abstract

Bicaudal D2 (BICD2) joins dynein with dynactin into a ternary complex (termed DDB) capable of processive movement. Point mutations in the *BICD2* gene have been identified in patients with a dominant form of spinal muscular atrophy, but how these mutations cause disease is unknown. To investigate this question, we have developed in vitro motility assays with purified DDB and BICD2's membrane vesicle partner, the GTPase Rab6a. Rab6a–GTP, either in solution or bound to artificial liposomes, released BICD2 from an autoinhibited state and promoted robust dynein–dynactin transport. In these assays, BICD2 mutants showed an enhanced ability to form motile DDB complexes. Increased retrograde transport by BICD2 mutants also was observed in cells using an inducible organelle transport assay. When overexpressed in rat hippocampal neurons, the hyperactive BICD2 mutants decreased neurite growth. Our results reveal that dominant mutations in BICD2 hyperactivate DDB motility and suggest that an imbalance of minus versus plus end–directed microtubule motility in neurons may underlie spinal muscular atrophy.

Introduction

Eukaryotic cells rely on the activities of plus- and minus-end-directed microtubule motors for proper function and maintenance. The retrograde motor, cytoplasmic dynein, is involved in a host of cellular activities, including the trafficking of diverse cargos such as organelles, vesicles, and mRNA as well as mitotic spindle alignment and chromosome positioning (Allan, 2011). In contrast to yeast dynein, which can achieve long-range transport on its own (Reck-Peterson et al., 2006), mammalian dynein must form a tripartite complex with the 1.2 mDa dynactin complex and an adapter protein to move processively along microtubules (McKenney et al., 2014; Schlager et al., 2014b).

A number of different adaptor proteins that join dynein and dynactin into an active motile complex have been identified (McKenney et al., 2014; Cianfrocco et al., 2015). In addition to enabling the formation of a dynein-dynactin complex, these adapters bind to receptors located on distinct cargos within the cell. For example, Bicaudal D2 (BICD2), one of best studied dynein adaptors, interacts with the small GTPase Rab6, which is found on early endosomes and ER-Golgi vesicles (Matanis et al., 2002). Rab6 also may play an important role in regulating the ability of BICD2 to interact with dynein and dynactin. BICD2 is thought to be auto-inhibited through an interaction between its C-terminal coiled-coil domain (CC3) with the N-terminal domain of the protein, which prevents it from associating with its other partners, including dynein (Matanis et al., 2002; Hoogenraad et al., 2003; Liu et al., 2013). Auto-inhibition is thought to be relieved by

binding to an effector, such as Rab6a in its GTP-bound form (Liu et al., 2013); however, evidence for this model is lacking.

BICD2 recently emerged as a genetic locus associated with spinal muscular atrophy (SMA), a genetic disorder characterized by the degeneration of anterior horn cells and leading to eventual muscle atrophy and weakness. The most common form of SMA is recessive in nature and is caused by mutations in the survival motor neuron gene, affecting 1 in 10,000 live births each year (Dimitriadi et al., 2016). Genetically dominant forms of the disease also have been identified. Recent studies on autosomal-dominant congenital spinal muscular atrophy (DCSMA) have identified a handful of mutations in BICD2 that are associated with the disease (Neveling et al., 2013; Oates et al., 2013; Peeters et al., 2013). The effects that these point mutations have on BICD2's ability to function as a dynein adaptor are not known, although overexpression of these mutants has been reported to cause Golgi fragmentation and changes in BICD2 localization in cultured cells (Neveling et al., 2013; Peeters et al., 2013). Interestingly, point mutations in the tail region of heavy chain 1 of cytoplasmic dynein have been associated with another form of spinal muscular atrophy, SMA-LED1. These mutations were reported to cause an increase in the affinity between the motor and BICD2 (Peeters et al., 2015) and a decrease in dynein-dynactin processivity (Hoang et al., 2017).

Here, we utilize a combination of biochemical and single-molecule in vitro motility assays to compare the behaviors of wild-type and mutant BICD2. We demonstrate that

Rab6a in its GTP-bound form enhances the formation of motile mammalian dynein/dynactin/BICD2 (DDB) complexes. BICD2 mutations associated with human disease cause a gain-of-function in motility, allowing more DDB complexes to form and move along microtubules both in vitro and in vivo. In addition, we show that the expression of BICD2 mutants in neurons leads to impaired neurite outgrowth. These results indicate that the SMA BICD2 mutants hyperactivate dynein motility, a gain-of-function consistent with a dominant genetic trait. An increase in retrograde over anterograde transport in neurons could explain the gradual loss of motor neuron function in SMA.

Results

Activation of BICD2 via Rab6a-GTP increases dynein-dynactin binding and motility

Bicaudal D2 is comprised of five coiled-coil domains that can be grouped into three distinct regions (Fig. 1A). The C-terminal region of the protein is the most well-conserved and contains the binding site to different partners localized to different cargos, including the small GTPase Rab6a (Matanis et al., 2002). An N-terminal construct of the protein, which spans residues 25-400 (BICD2$_{25-400}$), was shown to be more effective in binding dynein-dynactin in cell lysate pull-down assays compared to autoinhibited full-length protein (BICD2$_{FL}$) (Splinter et al., 2012b; McKenney et al., 2014). We replicated these findings; the difference in dynactin binding was especially striking, exhibiting about a

10-fold reduction for the BICD2$_{FL}$ pull-down compared with BICD2$_{25-400}$, while dynein was ~2-3 fold lower (Supp. Fig. 1A and 1B).

We next tested whether the auto-inhibited state of BICD2$_{FL}$ could be activated by Rab6a. We added purified recombinant Rab6a-Q72L, which is locked in a GTP-bound state (hereon referred to as Rab6a^{GTP}), to porcine brain lysate and performed pull-downs using BICD2 as bait (Matanis et al., 2002). With increasing Rab6a^{GTP}, there was a corresponding increase of dynein and dynactin in the BICD2$_{FL}$ pull-down. Conversely, the GDP-bound mutant of Rab6a (Rab6a-T27N, hereon Rab6a^{GDP}) appeared to somewhat reduce the pull-down of dynein and dynactin (Fig. 1B). Rab6a^{GTP} also was detected in the pellet fraction in these experiments, whereas Rab6a^{GDP} was absent (Supp. Fig. 1C). A densitometric analysis shows a ~2.5-fold increase in dynein enrichment and a ~10-fold increase in dynactin at the highest Rab6a^{GTP} concentration used (Supp. Fig. 1D). The greater pull-down of dynactin relative to dynein might reflect an interaction of the Rab6a^{GTP}-BicD2 complex with dynactin alone. Together, these results indicate that Rab6a^{GTP} is able to activate full-length BICD2 and enhance its ability to bind to dynein and dynactin.
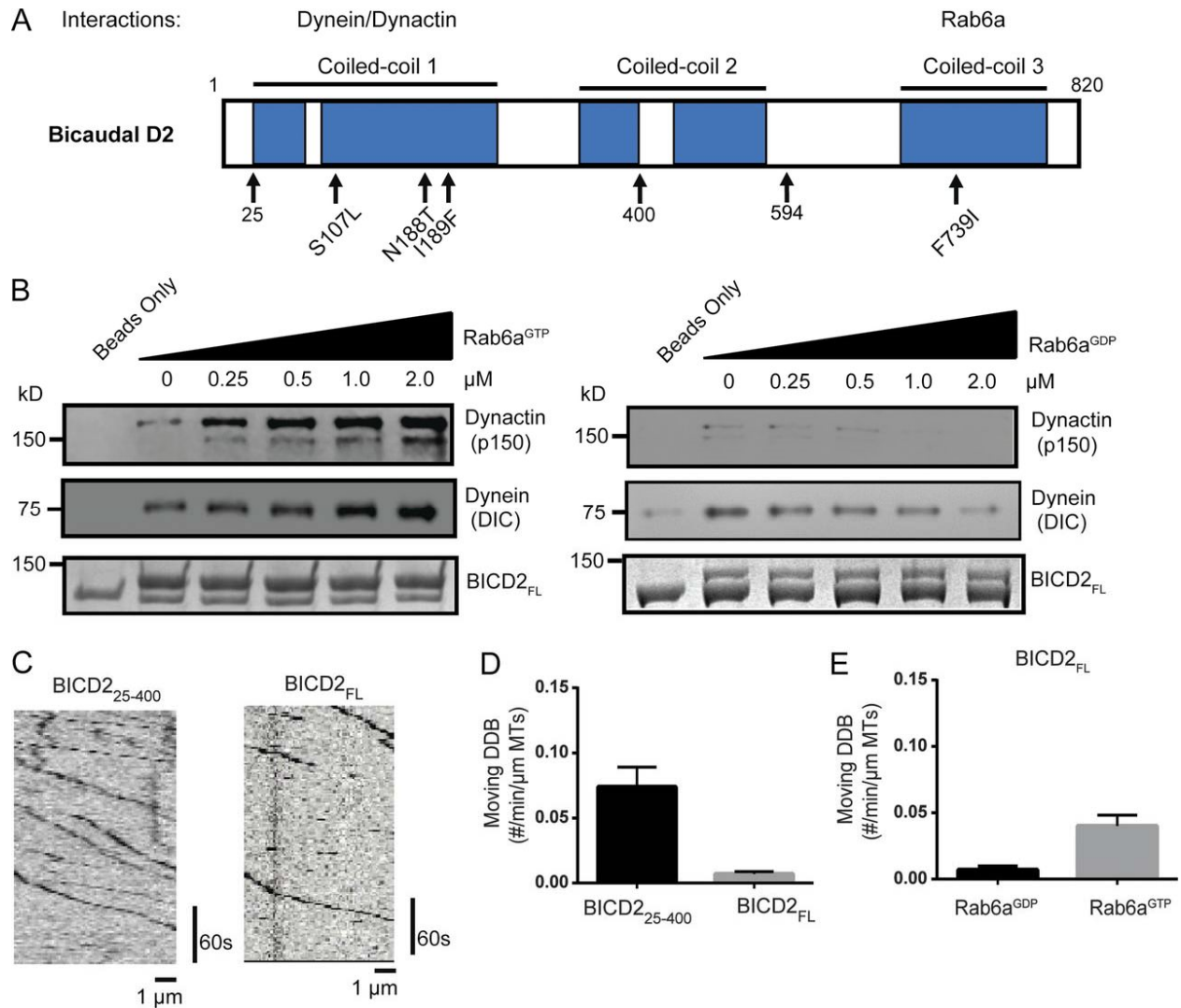
Figure 1. BICD2_FL activation by Rab6a^GTP

(A) Domain architecture of mammalian Bicaudal D2. N188T, I189F, and S107L are mutations associated with human SMA-LED, and F739I is the analogous mutation to the classical Drosophila mutation F684I. Amino acids 400 and 594 indicate the end of constructs used in this study. (B) Porcine brain lysate pull-down using full-length (FL) BICD2 as bait. Increasing amounts of recombinant Rab6a^GTP (left) or Rab6a^GDP (right) were added to the lysate, and the amount of endogenous dynein (dynein intermediate chain

[DIC]) and dynactin (p150 subunit) bound was analyzed by immunoblot. (C) Sample kymographs of single-molecule DDB (aa 25–400 or FL BICD2) motility on microtubules. Fluorescence is from the N-terminal sfGFP tag on BICD2. (D) Quantification of the number of moving motors per micrometer of microtubule; mean and SEM from n = 3 independent experiments (each experiment measuring a minimum of 30 microtubules). (E) Quantification of number of moving motors per micrometer of microtubule of BICD2$_{FL}$ with either Rab6a^{GDP} or Rab6a^{GTP} added; mean and SEM from n = 3 independent experiments (each experiment measuring a minimum of 30 microtubules).

To further examine whether Rab6a^{GTP} can activate BICD2$_{FL}$ and enable dynein-dynactin motility, we utilized total internal reflection microscopy (TIRF) to visualize DDB motility on microtubules. Purified dynein and dynactin from mammalian RPE-1 cell lysates were incubated with equimolar concentrations of either superfolder-GFP (sfGFP)-fused BICD2$_{25-400}$ or BICD2$_{FL}$, and the numbers of moving motor complexes were analyzed via kymographs (Fig. 1C). This single molecule in vitro assay revealed that the truncated BICD2$_{25-400}$ produced more processive dynein-dynactin complexes when compared to BICD2$_{FL}$, which is again consistent with the idea that BICD2$_{FL}$ is autoinhibited (Fig. 1C, 1D, Supp. Video 1). The addition of Rab6a^{GTP} to BICD2$_{FL}$ and dynein-dynactin resulted in a 3-4-fold increase in the number of moving DDB$_{FL}$ complexes on microtubules compared to Rab6a^{GDP} or the individual DDB components alone (Fig. 1E). In contrast, Rab6a^{GTP} neither increased the motility of DDB$_{25-400}$ (Supp. Fig. 1E) nor interacted with BICD2$_{25-400}$ (Supp. Fig. 1F). Collectively, these results suggest that Rab6a^{GTP} is capable of alleviating the auto-inhibition of full-length BICD2 and activating its ability to form processive DDB complexes.

Disease-related point mutations in BICD2 increase binding to dynein/dynactin and motility

Next, using our assay, we sought to examine the effects of three BICD2$_{FL}$ mutants identified in patients afflicted with DC-SMA/SMA-LED2 (S107L, N188T, I189F) and a mutant (F739I) that is equivalent to the *Drosophila* F684I mutant that produces a bicaudal

phenotype (Fig. 1A) (Wharton and Struhl, 1989; Mohler and Wieschaus, 1986). The latter mutation has been shown to have higher affinity towards dynein as compared to wild-type and was proposed to be more readily activated upon binding to cargo (Liu et al., 2013). All four of the mutated residues are highly conserved in the BICD protein family.

In a brain lysate pull-down assay with Rab6a^{GTP}, the four BICD2$_{FL}$ mutants recruited more dynein and dynactin compared to wild-type BICD2$_{FL}$, with the greatest difference being observed in dynactin binding (Fig. 2A, Supp. Fig. 2B). Weak binding of dynein-dynactin also was observed with Rab6a^{GDP} or without Rab6 (Fig. 2A, 2B, Supp. Fig. 2B). It is possible that endogenous Rab6a^{GTP} in the brain lysate might be responsible for this weak BicD2 mutant-specific pull-down or that other factors in the lysate allow for a loss of autoinhibition. In the single molecule TIRF assay in the presence of Rab6a^{GTP}, three of the BICD2$_{FL}$ mutants (N188T, I189F, S107L) showed a statistically significant 20-30% increase in the number of motile DDB compared to wild-type BICD2$_{FL}$ (Fig. 2C). Neither the velocity (Fig. 2D) nor run-length of DDB (Fig. 2E, Supp. Fig. 2C) was different between wild-type and mutant BICD2$_{FL}$. In the presence of Rab6a^{GDP}, however, motility was much lower and no statistical difference was observed between mutant and wild-type BICD2$_{FL}$ (Supp. Fig 2D). No significant difference also was observed in the number of motile DDB complexes formed by wild-type and mutant truncated BICD2$_{25-400}$ (Fig. 2F). Wild-type and mutant BICD2$_{25-400}$ also pulled down similar amounts of dynein and dynactin (Supp. Fig. 2E). Collectively, these results indicate the point mutations in

BICD2_{FL} enhance Rab6a^{GTP}-dependent activation from the auto-inhibited state, producing more motile DDB_{FL} complexes, while not altering the measured parameters of DDB_{FL} motility.
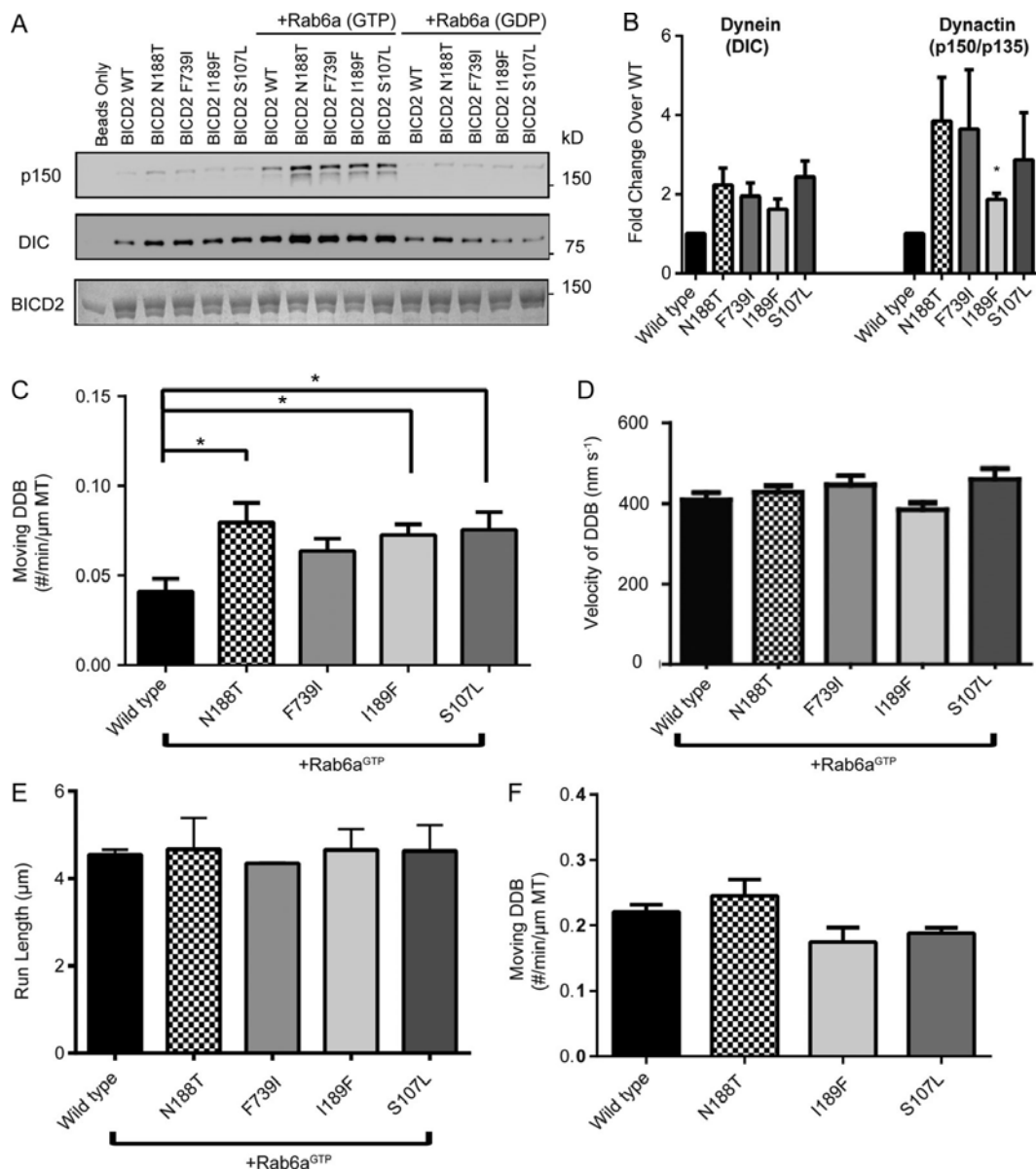
**Figure 2. BICD2FL mutants show increased binding to dynein/dynactin and single-molecule motility in vitro**

(A) Porcine brain lysate pull-down using BICD2FL as bait. Rab6aGTP or Rab6aGDP was

added to the lysate at a concentration of 1 μM. The amount of endogenous dynein (DIC)

and dynactin (p150 subunit) bound was analyzed by immunoblot. The amount of

BICD2 on beads was visualized using Coomassie stain. (B) The ratio of dynein or

dynactin band intensity for mutants compared with WT BICD2 for the lysate only

condition; mean and SEM from n = 3 independent experiments. Mean, SEM, and p-values for the mutants shown for DIC are as follows: N188T: 2.24 ± 0.42, P = 0.10; F739I: 1.95 ± 0.34, P = 0.11; I189F: 1.61 ± 0.27, P = 0.15; and S107L: 2.44 ± 0.41, P = 0.07. Mean, SEM, and p-values for p135/p150 are as follows: N188T: 3.86 ± 1.09, P = 0.12; F739I: 3.65 ± 1.5, P = 0.22; I189F: 1.88 ± 0.14, P = 0.027; and S107L: 2.88 ± 1.18, P = 0.25. Quantitation of the other conditions are shown in Fig. S2 (A and B). (C) Dynein and dynactin (purified from RPE-1 cells; see Materials and methods) were incubated with BICD2 and flowed into a motility chamber. The number of moving DDB motors, as visualized by sfGFP fluorescence on BICD2, was quantified per minute per micrometer length of microtubules in the assay; mean and SEM from n = 3 independent experiments (each experiment measuring a minimum of 30 microtubules); *, P ≤ 0.05. (D) Velocities of the moving motors from C is shown; mean and SEM from n = 3 independent protein preparations and experiments (each experiment measuring a minimum of 100 DDB complexes). (E) The run lengths of WT and mutant DDB$_{FL}$; mean and SEM from n = 3 independent experiments (each experiment measuring a minimum of 130 DDB complexes). For processivity measurements, the NaCl concentration was increased from 50–65 mM to reduce the run length so that it could be more reliably measured (see Materials and methods). (F) Purified dynein and dynactin were incubated with truncated BICD2$_{25-400}$ (WT and mutant) and flowed into a motility chamber. The number of moving DDB complexes, as visualized by SNAP-TMR fluorescence on BICD2, was

25

quantified per minute per micrometer of microtubule; mean and SEM from n = 3

independent protein preparations and experiments (each experiment measuring a

minimum of 30 microtubules).

A liposome assay provides an in vitro system for cargo transport

The retrograde transport of native membranous cargos (Grigoriev et al., 2007; Utskarpen et al., 2006) involves prenylated, membrane-bound Rab6a interacting with BICD2. We sought to recapitulate this cargo motility in vitro using recombinant Rab6a^{GTP} or Rab6a^{GDP} covalently linked to large unilamellar vesicles (LUVs) via maleimide lipids (Fig. 3A). With Rab6a^{GTP} on the liposomes, we observed the frequent binding and movement of liposomes along microtubules in the presence of dynein, dynactin, and BICD2$_{FL}$ (Fig. 3B, 3C). In contrast, motility events were only rarely observed on Rab6a^{GDP}-coated liposomes (Fig. 3B, 3C, Supp. Video 2). Next, we examined the BICD2$_{FL}$ mutants in the Rab6a^{GTP} liposome motility assay. All four mutants produced significantly more moving Rab6a^{GTP} liposomes compared to wild-type BICD2$_{FL}$ (Fig. 3D). The velocities of wild-type and mutant BICD2 were similar (~500 nm/s; (Supp. Fig. 2F)) and slightly higher than the single molecule velocities. Thus, consistent with the single-molecule motility assays, the BICD2 mutants hyper-activated dynein-dynactin motility in an in vitro cargo transport assay.
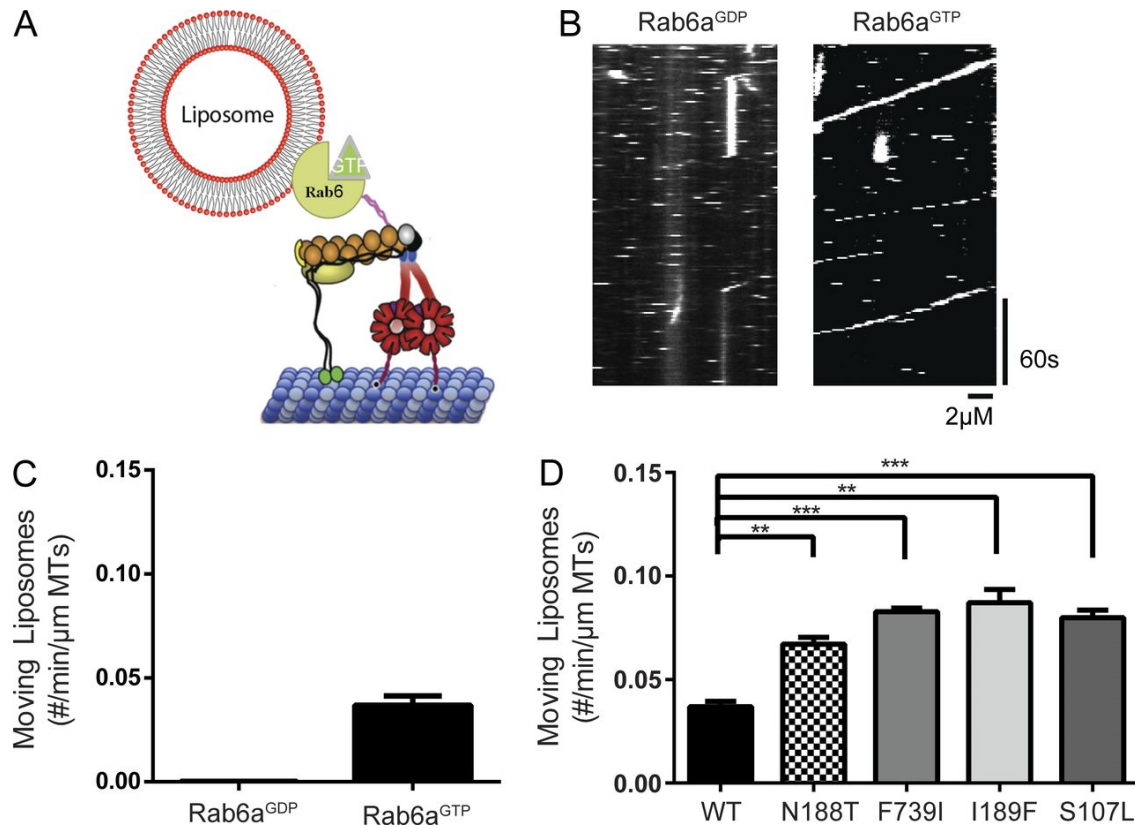
Figure 3. A motility assay using liposomes recapitulates single-molecule data

(A) A schematic of the liposome motility assay. Rab6a was conjugated to maleimide lipids incorporated into 200-nm-sized liposomes and incubated in solution with DDB. Liposomes were labeled with 0.1% rhodamine–PE. (B) Representative kymographs of Rab6aGDP versus Rab6aGTPliposomes moving along microtubule in the presence of DDBFL. Horizontal dashed lines represent liposomes transiently entering the field of focus. (C) Quantification of number of motile Rab6aGDP or Rab6aGTP liposomes when incubated with DDBFL; mean and SEM from n = 3 independent experiments (each experiment measuring a minimum of 30 microtubules; runs for Rab6aGDP occurred very infrequently). (D) Quantification of the number of motile Rab6aGTP liposomes moving

on microtubules when incubated with DDBFL (WT vs. mutant); mean and SEM from n =

3 independent experiments (each experiment measuring a minimum of 30 microtubules);

**, P ≤ 0.01; ***, P ≤ 0.001.

Enhanced retrograde motility induced by BICD2 mutants in a cell-based assay

To examine the behavior of wild-type and mutant BICD2 in cells, we turned to a previously established inducible cargo trafficking assay (Hoogenraad et al., 2003; Kapitein et al., 2010). In this assay, FRB-BICD2 is co-expressed with FKBP fused to a peroxisome localization sequence (Fig. 4A). As shown previously, an N-terminal construct of BICD2 (FKBP-BICD2$_{1-594}$) in the presence of rapamycin increased retrograde transport of peroxisomes and produced significant clustering of the GFP-peroxisome signal around the perinuclear region (Hoogenraad et al., 2003) (Fig. 4B). This longer construct includes part of coiled-coil 2, but still lacks the C-terminal region needed for autoinhibition. In contrast, the autoinhibited FKBP-BICD2$_{FL}$ construct displayed a more dispersed peroxisome signal (Fig. 4B).

We next tested the mutant BICD2$_{FL}$ constructs in this inducible peroxisome motility assay. To quantify the degree of peroxisome clustering due to minus-end-directed motility, we used a previously created software (ICY) that calculates the fraction of the cell area containing 90% of the total peroxisome GFP signal; increased transport to the centrosome results in a more clustered signal and thus 90% of the signal occupies less area (de Chaumont et al., 2012; Mounier et al., 2012) (Fig. 4C). In the absence of rapamycin, the clustering values for the wild-type and mutants were similar (~55%; Fig. 4D). With the addition of rapamycin to cells expressing BICD2$_{1-594}$, the peroxisomes occupied ~20% of the cell area compared with ~40% expressing auto-inhibited BICD2$_{FL}$.

The four mutants tested in the BICD2$_{FL}$ construct, while not achieving the same degree of peroxisome clustering observed for BICD2$_{1-594}$, showed an increase in the compaction of the peroxisome signal compared to wild-type BICD2$_{FL}$ (Fig. 4D). Thus, similar to the in vitro data, the mutant BICD2$_{FL}$ proteins hyperactivated dynein-dynactin in a cellular context and more efficiently transported peroxisomes towards the centrosomes.
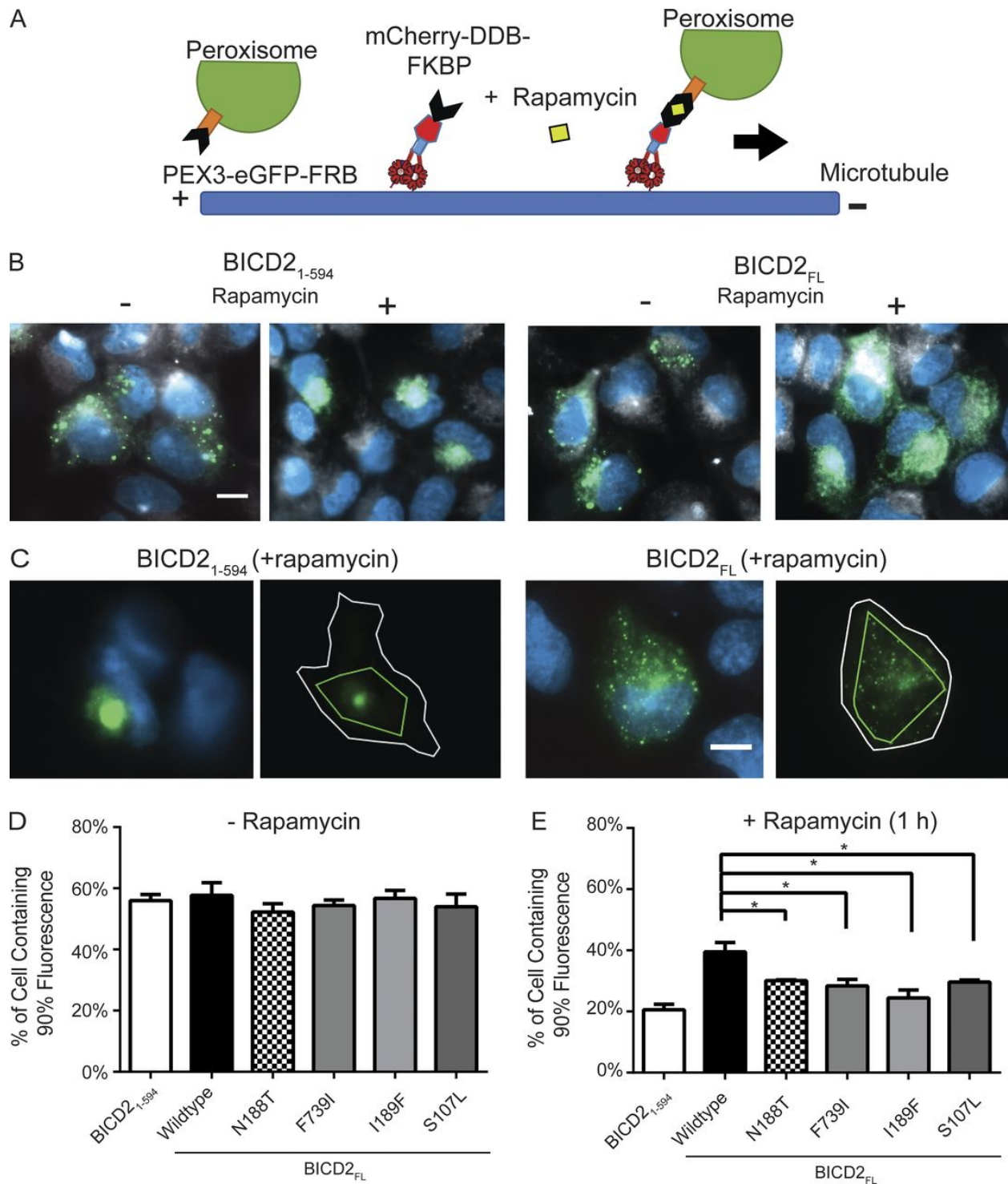
Figure 4. Cellular dynein–dynactin motility induced by WT and mutant BICD2

(A) Schematic of the cell-based peroxisome motility assay. U2OS cells were cotransfected

with a plasmid expressing GFP–FRB with a PEX3 localization sequence, targeting the
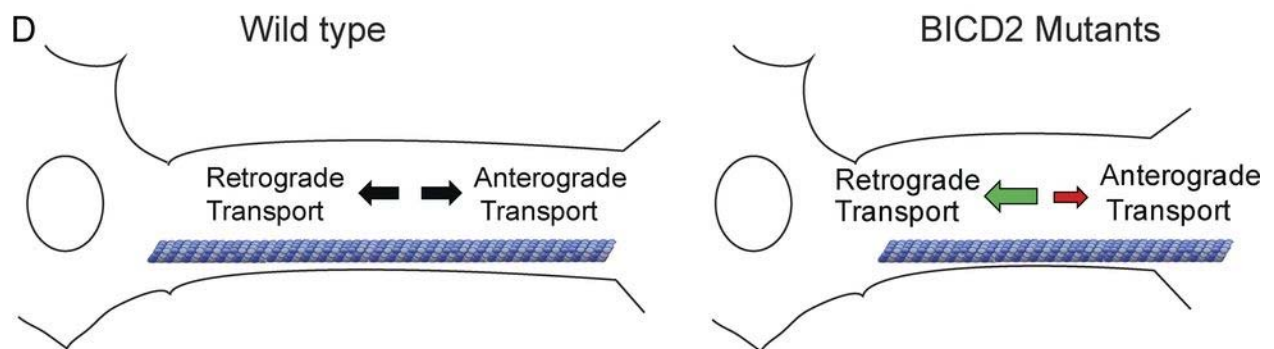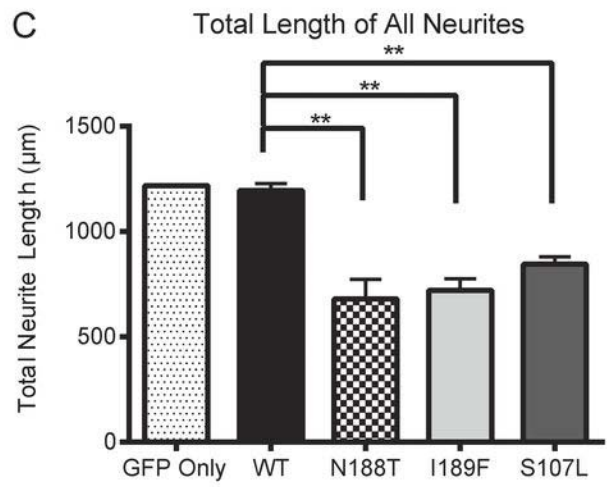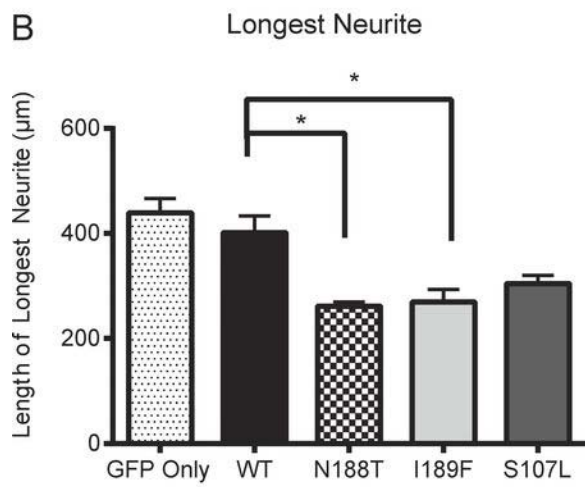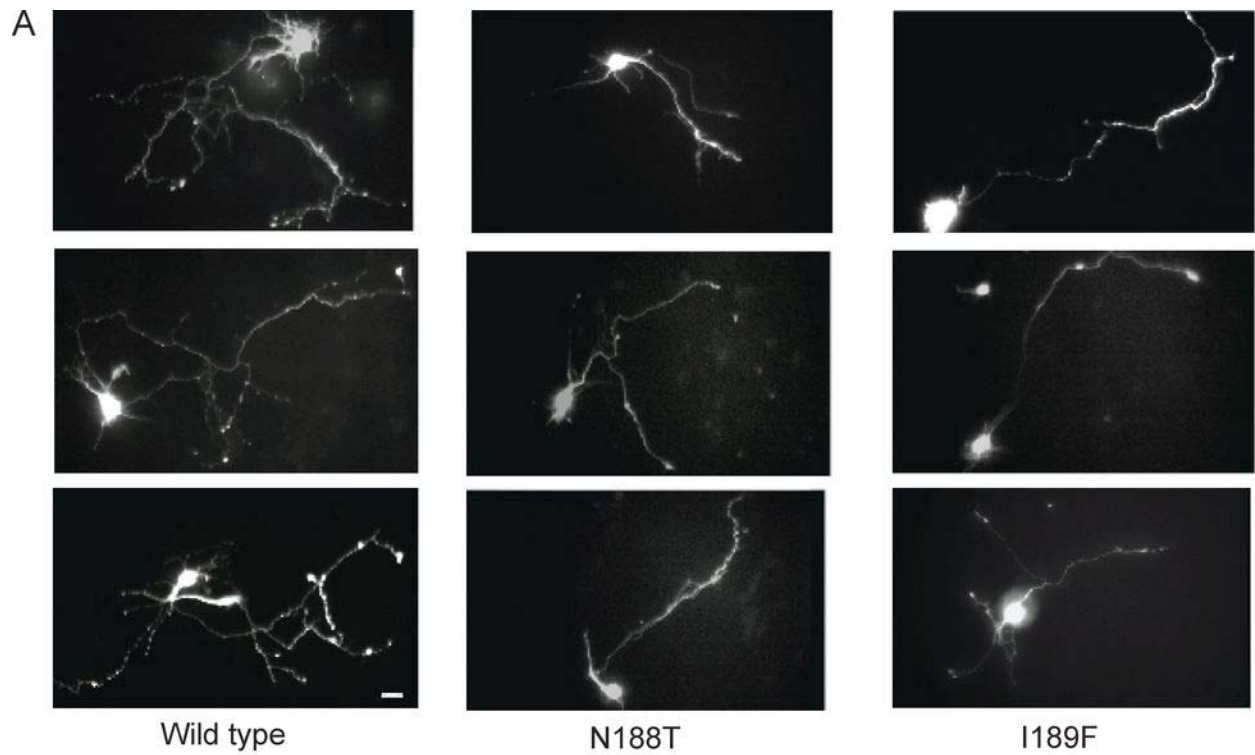
protein to peroxisomes, and an mCherry-BICD2–FKBP construct. After addition of rapamycin, mCherry-BICD2–FKBP is recruited to peroxisomes. If in an active state, the BICD2 recruits dynein–dynactin, which transport the peroxisome along microtubules toward the centrosome. (B) Representative epifluorescence images of the assay for both BICD2$_{1-594}$ and BICD2$_{FL}$. Peroxisomes are shown in green, the white signal represents the far-red cell membrane marker, CellMask, and blue is DAPI. In the absence of rapamycin, peroxisomes decorated with GFP–FRB are distributed throughout the cytoplasm (columns 1 and 3). 1 h after rapamycin addition, peroxisomes in cells expressing BICD2$_{1-594}$ are heavily clustered at the cell center (column 2), whereas those expressing BICD2FL exhibit less clustering (column 4). Bar, 10 µm. (C) Example image of an analyzed cell for both BICD2$_{1-594}$ and BICD2$_{FL}$. The white outline depicts the cell boundary; the inner green line indicates the area that contains 90% of fluorescence (see Materials and methods). Bar, 10 µm. (D and E) Quantification of the cell clustering data. The percentage of the cell area in which 90% of total fluorescence was contained is used as a measure for the degree of clustering (see Materials and methods). Lower values reflect a higher degree of clustering; mean and SD from n = 3 independent experiments (each experiment measuring a minimum of 25 cells for each construct); *, P ≤ 0.05.

We also tested whether localizing Rab6a^{GTP} containing a peroxisome targeting sequence (Rab6a^{GTP}-PEX) could increase the activity of FKBP-BICD2$_{FL}$. However, we found that Rab6a^{GTP}-PEX alone (without FKBP-BICD2$_{FL}$ co-expression) was sufficient to cluster peroxisomes, presumably through the recruitment of endogenous BICD2 and then dynein-dynactin (Supp. Fig. 3A, 3B, 3C). Thus, targeting of Rab6a^{GTP} on peroxisome membranes is sufficient for the recruitment and activation of endogenous BICD2 to produce dynein-mediated transport of peroxisomes.

Over-expression of BICD2 mutants in hippocampal neurons decreases neurite length

We next tested whether the hyperactivating BICD2$_{FL}$ mutants affected neurite outgrowth and morphology of neurons. Rat hippocampal neurons, dissected from embryonic day 18 tissue and grown in culture, were transfected with either wild-type or mutant mouse mCherry-BICD2$_{FL}$ constructs along with soluble GFP to visualize the cell body and neurites (Fig. 5A). Three days later, dual mCherry and GFP positive neurons were then scored for the length of their longest process as well as the total length of all processes. Cells transfected with wild-type mCherry-BICD2$_{FL}$ and GFP showed similar neurite lengths compared to cells transfected with GFP alone (Fig. 5B, 5C). This result is consistent with previous work showing that over-expression of wild-type BICD2 in either hippocampal or rat DRG neurons does not affect axon length or overall neurite length (Schlager et al., 2014c). However, cells transfected with the disease-mutant BICD2$_{FL}$ constructs for three days showed a ~40% decrease in both the length of the longest neurite

34

as well as an overall decrease in total neurite length after three days in culture (Fig. 5B, 5C). This result is similar to what was reported when the BICD-related protein, BICDR-1, which forms a higher velocity DDB complex, is over-expressed in neurons. (M. A. Schlager, Serra-Marques, et al., 2014; M. A. Schlager et al., 2010). The number of long (>15 m) processes emanating from the cell body was not affected by the BICD2 mutants (Supp. Fig. 3D). The Drosophila mutant (F739I) also showed a significant reduction in total neurites, but not in the axon length (Supp. Fig. 3E, 3F). These results demonstrate that mutations in BICD2 affect the process of neurite outgrowth of hippocampal neurons in culture.

A

Wild type   N188T   I189F

B **Longest Neurite**

C **Total Length of All Neurites**

D **Wild type**   **BICD2 Mutants**

Retrograde Transport ← → Anterograde Transport

Retrograde Transport ← → Anterograde Transport

Figure 5. Overexpression of BICD2 mutants in rat hippocampal neurons results in a decrease in neurite length.

(A) Representative images of hippocampal neurons overexpressing mCherry–BICD2$_{FL}$ (WT and mutants) or an empty plasmid control; neurons were also co-transfected with soluble GFP in order to mark the neurites. Bar, 10 µm. (B) Axon length after 3 d of overexpression of BICD2$_{FL}$ constructs; mean and SD from n = 3 independent experiments (each experiment measuring 15–20 neurons for each construct); *, P ≤ 0.05. (C) Total neurite length after 3 d of overexpression of BICD2$_{FL}$ constructs; mean and SD from n = 3 independent experiment (each experiment measuring 15–20 neurons for each construct); **, P ≤ 0.01. (D) Model of how a gain of function in dynein-based motility from BICD2 mutants might cause an imbalance in axonal transport and lead to SMA. See Discussion for more details.

Discussion

In this study, we developed in vitro single-molecule and liposome assays that recapitulate Rab6a^{GTP}–dependent activation of DDB motility. These assays revealed that three BICD2 mutants identified in patients afflicted with DC-SMA/SMA-LED2 (S107L, N188T, I189F) and one mutant that emerged from a *Drosophila* screen (F739I in our mammalian construct) all display a similar phenotype of eliciting more moving DDB complexes. These general findings of dynein activation were further substantiated in cells with a regulated BICD2 recruitment assay to peroxisomes. Interestingly, this effect of these human disease mutants was not evident with the Rab6a-independent, constitutively active BICD2$_{25-400}$ construct, suggesting that the mutants have minimal effect on the stability or conformation of the DDB complex. Rather, our data is most consistent with a model in which the mutants lower the energy barrier for Rab6a^{GTP} to convert the autoinhibited BICD2$_{FL}$ into an active conformation. Future work can test this model using assays that probe the conformational states of BICD2$_{FL}$.

Previous cell-based models have looked for effects of BICD2 mutants that might explain the dominant phenotype of spinal muscular atrophy. One study reported that BICD2 mutants cause Golgi fragmentation, a phenotype that is often produced by interference with dynein function such as with the overexpression of the dynamitin subunit of dynactin (Burkhardt et al., 1997; Harada et al., 1998; Neveling et al., 2013).

Golgi disruption is also suggested by the delocalization of Rab6a from a normal perinuclear focus to a diffusive signal in cell lines of afflicted patients (Unger et al., 2016).

These studies suggest that the disease mutants may have a dominant negative effect on dynein function. While we cannot rule out dominant negative effects that cannot be measured with our assays, our data rather suggest that the mutants produce a dominant positive effect leading to enhanced dynein cargo transport. The effects are somewhat subtle (~25% increase in motile DDB complexes), but in a motor neuron with an axon up to a meter long, such changes may be sufficient to disrupt normal cargo transport over time. To explain the SMA disease phenotype, we propose a model in which mutant BICD2 increases dynein activation and leads to an imbalance between anterograde and retrograde transport (Figure 5D). The shift towards dynein transport could produce a decrease in the delivery of cargo to the nerve terminal, which in turn could lead to a gradual decline in function of neurons with long axons. This general model is consistent with results from Schlager et al. with the BICD-related protein, BICDR-1 (M. A. Schlager, Serra-Marques, et al., 2014; M. A. Schlager et al., 2010). These investigators found that BICDR-1 expression caused the accumulation of Rab6a vesicles close to the centrosome, suggesting that BICDR-1, like our BICD2 mutants, increases dynein-driven retrograde transport. Similar to our results with BICD2 mutants, the over-expression of the wild-type BICDR-1 adapter protein resulted in a ~50% decrease in axon and total neurite length.

This model also is congruous with experimental data from transgenic animals expressing various BICD2 constructs. Mice that are BICD2 null possess a normal spinal cord and their motor neurons exhibit no evidence of abnormal retrograde transport (Jaarsma et al., 2014). While these mice die at around p30 and do experience motor function irregularities, their overall phenotype does not resemble that of SMA patients. This result suggests that the absence or inhibition of BICD2 activity cannot explain the disease etiology. In contrast, transgenic mice expressing the shorter, more active N-terminal construct of BICD2 were impaired in retrograde axonal transport and Golgi fragmentation, presumably through a dominant negative effect of activating dynein and dynactin without cargo and causing its accumulation in the cell body (Teuling et al., 2008). Curiously, however, these mice, which live up to two years, also did not develop any motor abnormalities. The phenotypic differences in mice expressing the N-terminal construct of BICD2 compared with haploid S107L, N188T, and I189F BICD2 mutations suggests that the C-terminus of the protein that interacts with cargo is necessary for contributing to the SMA disease phenotype.

Recently, a number of disease-related mutants in the human dynein heavy chain also have been examined for their effects on motility at the single-molecule level (Hoang et al., 2017). Many of the mutants, including three mutations associated with SMA, exhibited normal DDB complex formation and velocity, but displayed a ~60-70% reduction in processivity. These data are consistent with earlier research showing that

mutations (*Cra1* and *Loa*) in the heavy chain of cytoplasmic dynein that cause motor neuron disease in mouse models produce a decrease in dynein run length in vitro and an impairment of fast retrograde transport in axons (Hafezparast et al., 2003; Ori-McKenney et al., 2010). These results revealing a loss-of-function in dynein transport differ from those described for the SMA BICD2 mutants, which show no change in processivity and a gain-of-function increase in the amount of retrograde transport. Taken together, these studies on dynein and BICD2 mutations reveal multiple ways in which changes in motor activity can affect can affect the homeostasis and function of neurons.

Supplementary Figure 1. BICD2$_{25-400}$ recruits more dynein/dynactin compared to full-length BICD2.
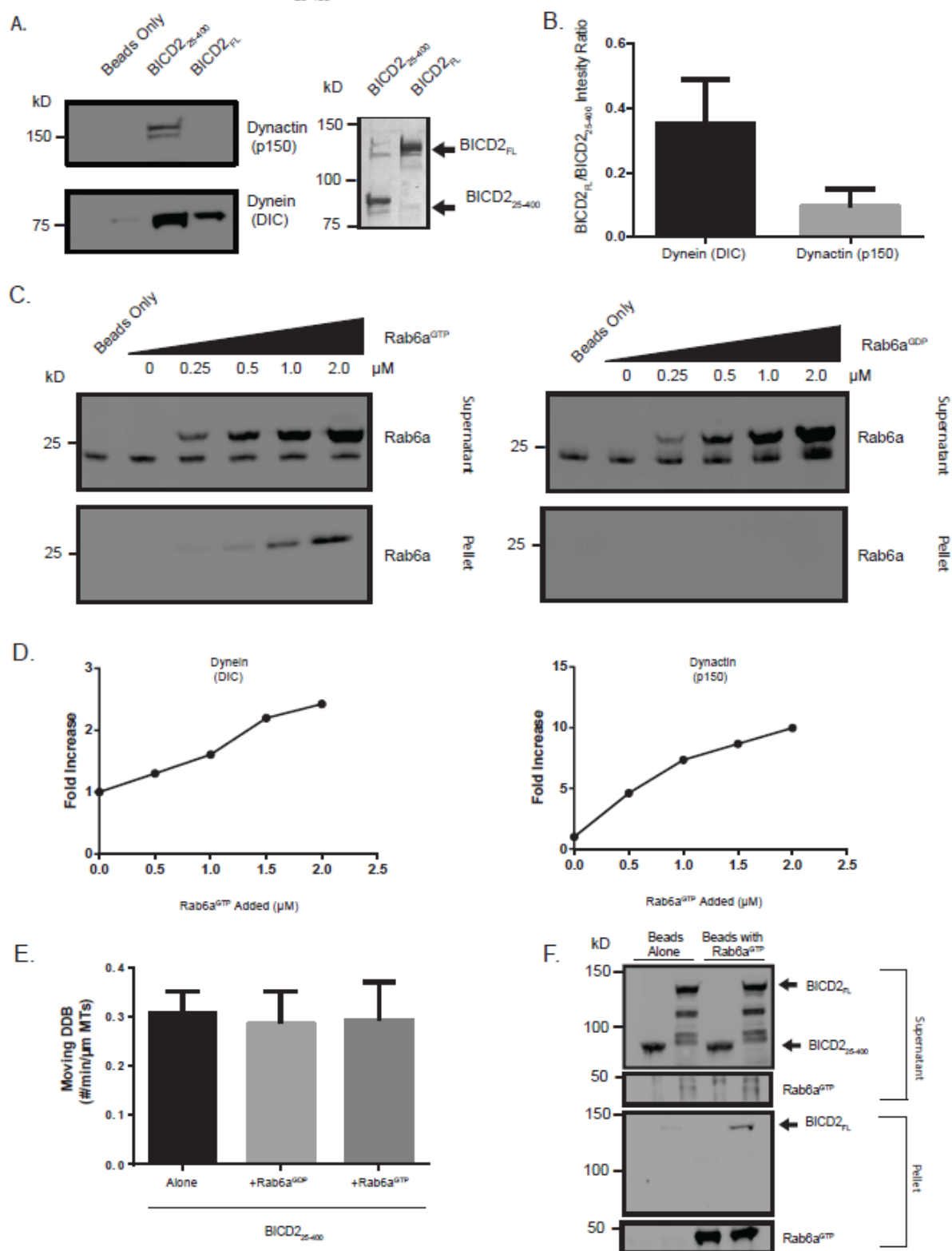
Fig. S1. BICD2$_{25-400}$ recruits more dynein as compared to full-length

 (A) A comparison of the amounts of dynein and dynactin pulled down from porcine brain lysate between BICD2$_{25-400}$ and BICD2$_{FL}$ **(B)** Quantification of the pull-down; mean and SD from n = 3 independent experiments. **(C)** The supernatant and pellet fraction of the pull-downs from Figure 1B showing that Rab6a^{GTP} but not Rab6a^{GDP} binds to the BICD2 on beads. **(D)** Quantification of the western blot shown in Figure 1B for the case of Rab6a^{GTP} addition. Values are normalized to the lane in which no Rab6a is added. **(E)** Quantification of number of moving motors per micron of microtubule of BICD2$_{25-400}$ with either no Rab6a added, Rab6a^{GDP} added, or Rab6a^{GTP} added; mean and SEM from n = 3 independent experiments (each experiment measuring a minimum of 30 microtubules). **(F)** GST-Rab6aGTP pull-down of either BICD2$_{25-400}$ or BICD2$_{FL}$.

Supplementary Figure 2. N-terminal mutant constructs of BICD2 exhibit no difference in dynein/dynactin binding.
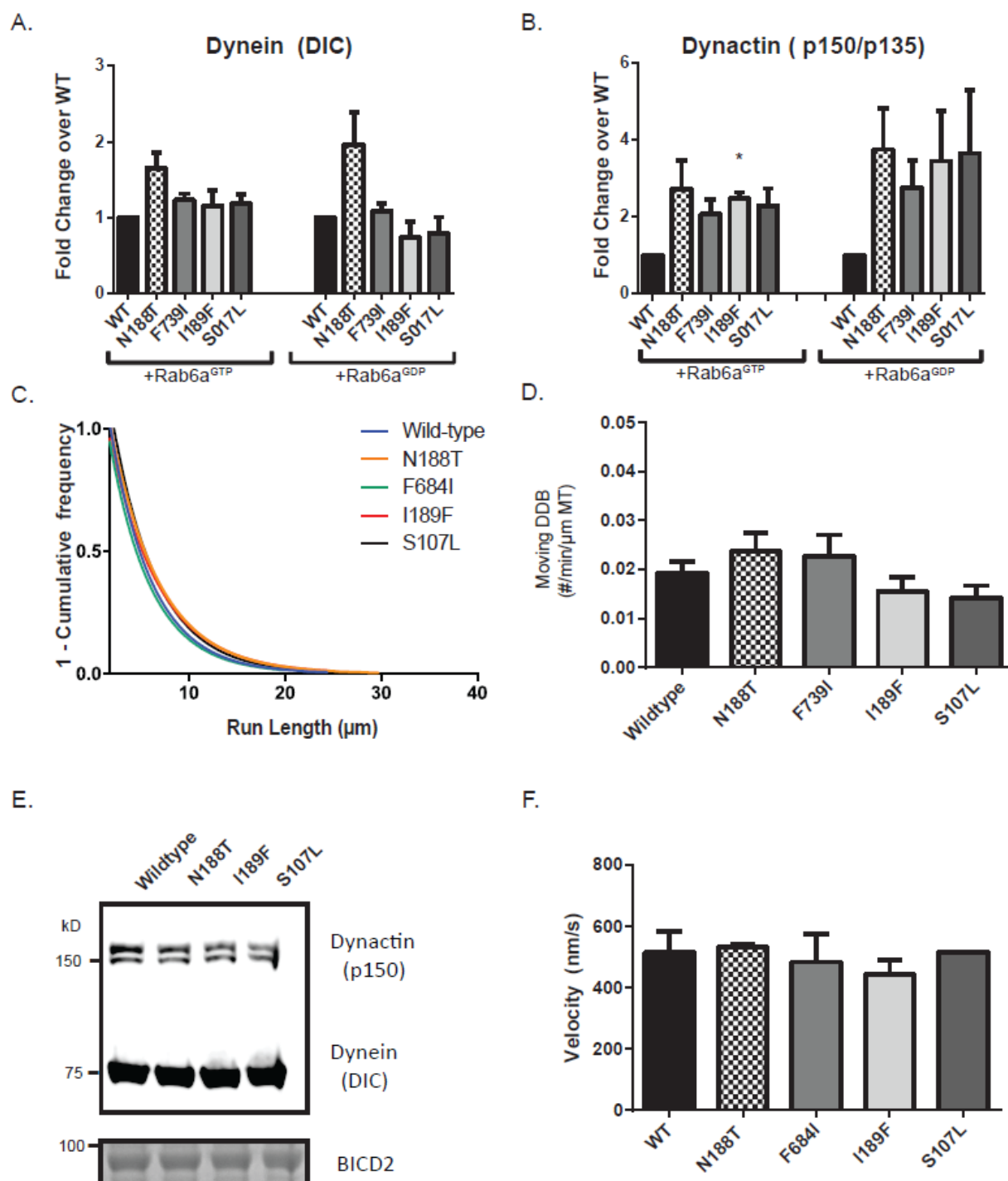
Fig. S2. **N-terminal mutant constructs of BICD2 are comparable to WT**

 (A) and **(B)** show the quantification of the western blots for Rab6a^{GTP} and Rab6a^{GDP} pull-downs from Figure 2; mean and SEM from n = 3 independent experiments. For (A), GTP addition mean and SEM are: N188T: 1.66 ± 0.20, p=0.082; F739I: 1.23 ± 0.082, p=0.11; I189F: 1.16 ± 0.20, p=0.51; S107L: 1.18 ± 0.12, p=0.26. GDP: addition N188T: 1.96 ± 0.42, p=0.15; F739I: 1.08 ± 0.097, p=0.47; I189F: 0.738 ± 0.21, p=0.34; S107L: 0.792 ± 0.21, p=0.43. For (B), GTP addition mean and SEM are: N188T: 2.71 ± 0.75, p=0.15; F739I: 2.06 ± 0.375, p=0.11; I189F: 2.48 ± 0.15, p=0.011; S107L: 2.28 ± 0.45, p=0.10. GDP: addition N188T: 3.75 ± 1.06, p=0.152 F739I: 2.75 ± 0.69, p=0.13; I189F: 3.44 ± 1.3, p=0.20; S107L: 3.65 ± 1.6, p=0.25. **(C)** Processivity data in the form of a 1-cumulative frequency histogram for one replicate, comparing different full-length BICD2 constructs. **(D)** The motility assay for DDB + Rab6a^{GDP} is also shown; mean and SEM from n = 3 independent experiments. **(E)** A comparison of BICD2$_{25-400}$ for WT and appropriate mutant constructs in the porcine brain lysate pull-down assay. Shown are the western blots of the pellet fractions for p150 and DIC and a Coomassie staining for BICD2. **(F)** Velocity measurements of liposomes shown in Figure 4D; mean and SEM from n = 3 independent experiments. Each experiment measured >100 liposomes. The error bar for S107L is too small to appear on the graph.

Supplementary Figure 3. Peroxisome-localized Rab6a^{GTP} is sufficient for clustering in cells
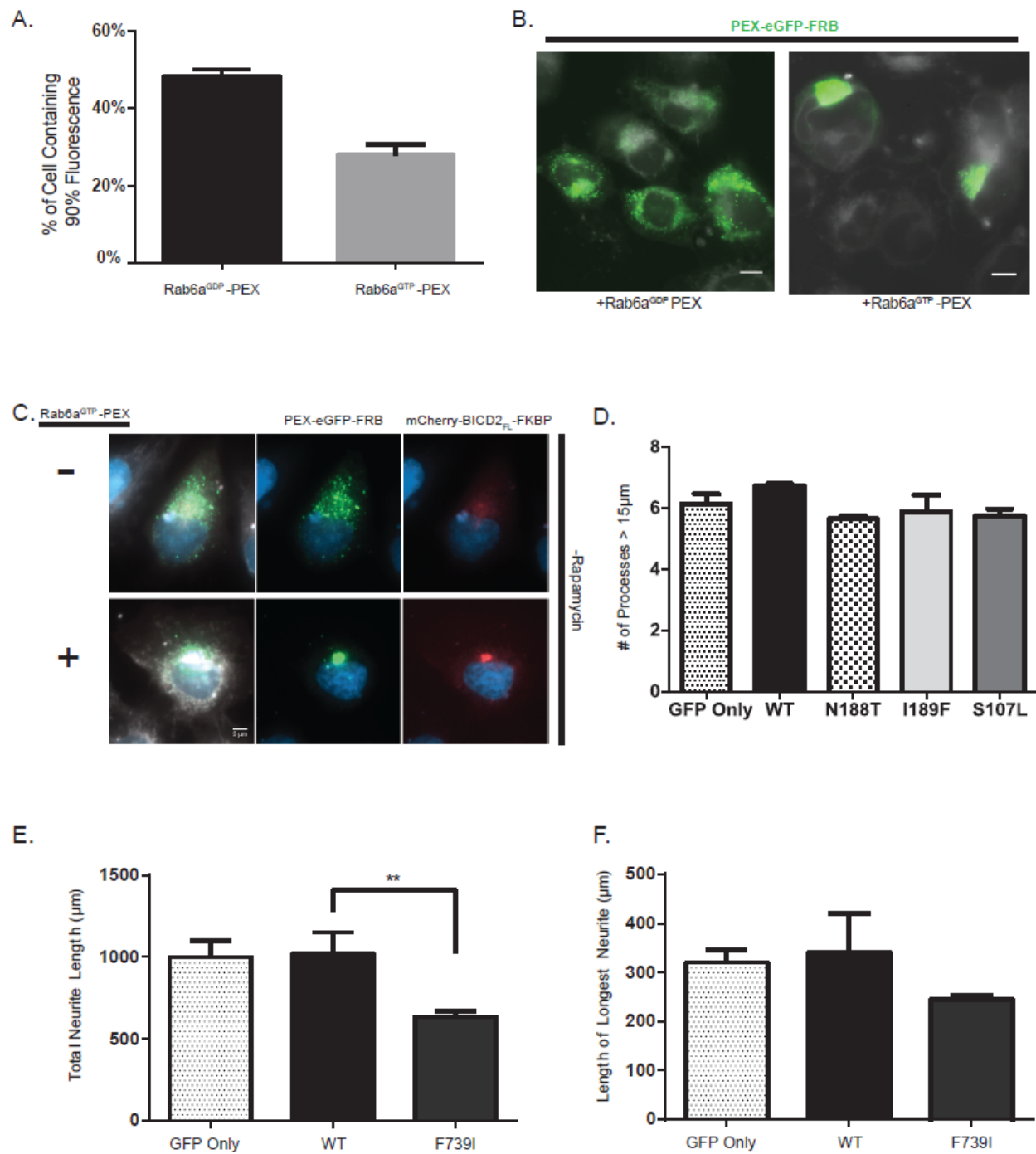
Fig. S3. Peroxisome-localized Rab6a^GTP is sufficient for clustering in cells

(A) A comparison of peroxisome clustering when either the GDP or GTP of Rab6a is fused with the PEX sequence; mean and SEM from n = 2 independent experiments. Each experiment measured at least 30 cells. **(B)** Representative images of peroxisomes from (A). The green color reflects PEX-eGFP-FRB, while the white is from a membrane dye. Scale Bar: 10 m **(C)** Example of BICD2_FL localizing to the peroxisomes even in the absence of rapamycin. In the top row, cells were transfected with PEX-eGFP-FRB and mCherry-BICD2_FL. In the bottom row, the cells were additionally transfected with Rab6a^GTP-PEX as well. **(D)** Quantification of total number of processes (> 15 m long) emanating from the cell body of the neurons from Figure 5a; mean and SD from n = 3 independent experiments. **(E)** Total neurite length after 3 days of over-expression of BICD2_FL constructs; mean and SD from n = 3 independent experiments (each experiment measuring 10-15 neurons for each construct) [**P ≤ 0.01]. **(F)** Axon length after 3 days of over-expression of BICD2_FL constructs; mean and SD from n = 3 independent experiments (each experiment measuring 10-15 neurons for each construct).

Material and Methods

DNA constructs

The cDNAs for mouse BICD2 (accession #AJ250106.1) and mouse Rab6a (accession #BC019118.1) were obtained from the Thermo Scientific MGC collection. BICD2 N-terminal constructs were cloned into a pet28a vector containing an N-terminal 6xHis-strepII-sfGFP tag. Full-length BICD2 WT and mutant constructs were cloned into a pFastbac vector containing either an N-terminal StrepII-sfGFP or StrepII-SNAPf tag followed by a C-terminal 6xHis tag for tandem purification. Rab6a was cloned into a pGEX vector containing an N-terminal GST tag followed by a PreScission protease cleavage site. The Rab6a constructs span the GTPase domain of Rab6a (a.a. 8-195), followed by a short linker and either a KCK motif for maleimide labeling purposes (liposome experiment), or a His10-tag. Point mutations for both the BICD2 constructs and the Rab6a GDP/GTP (Q72L and T27N, respectively) constructs were created by the protocol of Phusion, Inc.

For the cell-based peroxisome assay, the sequence spanning amino acids 1-42 of human PEX3 was synthesized via a gBlock (IDT), and was cloned into the N-terminal of a modified eGFP vector, followed by a C-terminal FRB sequence. BICD2 constructs for this assay were cloned into a pHR vector containing an N-terminal mCherry sequence and C-terminal FKBPf36v sequence. The Rab6a-PEX construct was constructed by fusing the

PEX3 sequence to the C-terminus of Rab6a lacking the cysteines for lipidation (1-203aa). A mTagBFP2 was fused to the N-terminus of this construct as well. For neuron expression, BICD2 was cloned into an N-terminal pmCherry vector.

Protein Purification

BICD2 N-terminal and Rab6a constructs were transformed into the *Escherichia coli* strain BL21 RIPL from Agilent. Cells were grown in LB at 37°C until growth reached ~0.6 OD_{280}. The temperature was then lowered to 18°C and cells were induced over-night with 0.5 mM IPTG. Bacterial pellets were resuspended in either strep lysis buffer (30 mM HEPES, pH 7.4, 300 mM NaCl, 2 mM $MgCl_2$, 5% glycerol, 5 mM DTT, 1 mM PMSF) for BICD2 or PBS containing 5% glycerol, 5 mM DTT, and 1 mM PMSF for Rab6a. Cells were lysed using an Emulsiflex press (Avestin) and clarified at 40,000g for 60 min. Lysates were bound to either Strep-tactin Superflow Plus resin (QIAGEN) or GST Sepharose 4B (GE Lifesciences). Beads were then washed extensively and the bound protein was eluted with 3 mM desthiobiotin in lysis buffer (BICD2) or via overnight cleavage with PreScission (Rab6a).

BICD2 full-length constructs were purified from SF9 cells and purified using tandem purification. Bacmids isolated from DH10Bac cells were transfected into SF9 cells. P2 virus was used to infect SF9 cells grown in shaker flasks to a density of $2x10^6$ cells/ml. After ~60 hr of infection, cells were harvested, pelleted, and resuspended in NiNTA lysis

buffer (30 mM HEPES pH 7.4, 300 mM NaCl, 5% glycerol, 20 mM imidazole, 1 mM PMSF, 5 mM βME) and lysed using an Emulsiflex. The lysate was clarified at 40,000g for 1 hr and bound to NiNTA resin from Qiagen. After extensively washing with lysis buffer, cells were eluted with lysis buffer containing 500 mM imidazole. The eluted material was then diluted to lower the imidazole concentration to 100 mM, and bound to Streptactin beads as described above. After elution, proteins were concentrated and injected onto either a Superose 6 10/300GL column (BICD2 constructs) or a S200 10/300GL column (Rab6a) from GE healthcare. Gel filtration buffer was comprised of: 30mM HEPES pH 7.4, 150mM NaCl, 10% glycerol, 2mM TCEP. Peak fractions were pooled and concentrated and then flash frozen. For SNAP-fusion constructs, purified proteins were bound to Streptactin beads and incubated at a 2:1 ratio of SNAP-TMR Star:Protein on ice for 1 hour. Beads were briefly washed in the gel filtration buffer and the protein was eluted with 3mM of desthiobiotin in gel filtration buffer.

Dynein and dynactin were prepared from RPE-1 cells. Fifteen 15cm dishes of RPE-1 cells were grown to ~80-900% confluency and then washed with PBS. The cells were then harvested using a cells scraper and pelleted at 500 x g for 5 minutes. They were then resuspended in 2.5mL of Buffer A (30 mM HEPES pH 7.4, 50 mM potassium acetate, 2 mM magnesium acetate, 1 mM EGTA, 10% glycerol) along with 5mM DTT, 1mM PMSF, and 1% Triton X-100 and incubated on ice for 10 minutes. The lysate was clarified at 266,000 x g and diluted to a volume of 25mL using Buffer A containing 1mM PMSF and

5mM DTT to reach a final Triton X-100 concentration of 0.1%. Streptactin sepharose (GE Healthcare) bound to purified StrepII-SNAP-FIP3 was added to the lysate and incubated for ~1 hour. The beads were then washed 4x with Buffer A containing 5mM DTT and 0.1% NP-40. Buffer A containing an additional 300mM NaCl was then added to the beads to form a 50% slurry and incubated on ice for 10 minutes to elute the dynein and dynactin bound to FIP3. This slurry was then passed through a 0.22μm filter to remove the beads. An equal volume of 50% Streptactin sepharose was added to this elution and allowed to gently mix for 30 minutes at 4°C to remove any remaining StrepII-SNAP-FIP3. The slurry was then filtered again and then diluted with Buffer A to reach a final NaCl concentration of 200mM. Sucrose was added to a final concentration of 6% and the dynein/dynactin were then flash frozen as aliquots.

Porcine Brain Pull-downs

Pull-downs were performed as previously described (McKenney et al., 2014). 500μl of clarified porcine brain lysate in Buffer A (30 mM HEPES pH 7.4, 50 mM potassium acetate, 2 mM magnesium acetate, 1 mM EGTA, 10% glycerol) was added to 80μl of a 50% suspension of Streptactin Sepharose beads (GE Healthcare) along with 100 nM of the BICD2 construct to be tested. To this, 0.1% of NP-40, 1 mM PMSF, and 5 mM DTT were added and the mixture was incubated at 4°C for 1 hr. The beads were then pelleted and washed 4 times with Buffer A containing 0.1% NP-40 and 5 mM DTT. The proteins were then eluted using SDS loading buffer and resolved on an acrylamide gel (Invitrogen). For

experiments where Rab6a was supplemented, the appropriate amount of recombinant Rab6a protein was added prior to the 4°C incubation step and processed in the same fashion.

Immunoblot Analysis

The SDS-PAGE gel was transferred onto a nitrocellulose membrane using the iBlot system from Invitrogen. Western blotting was performed using TBS buffer with 0.1% Tween-20 (TBS-T). Membranes were blot for 1 hr at room temperature with 5% milk in TBS-T, followed by a 1 hr primary antibody incubation. Antibodies used are as follows: mouse anti-p150 (clone 12, 1:250; BD), mouse anti-dynein intermediate chain (clone 74.1, 1:1000; EMD Millipore), mouse anti-6xHis (1:1000, Roche), mouse anti-Rab6a (ab55660, 1:500, Abcam). Membranes were washed 3x with TBS-T and then incubated with a secondary antibody for 1 hr at r.t. Secondary antibodies were: anti-mouse-800 or anti-rabbit-680 (1:10,000; Molecular Probes). Membranes were washed 3x with TBS-T and then imaged using an Odyssey Clx Infrared Imaging System (LI-COR Biosciences). Quantification of band intensity was performed using ImageJ's (NIH) gel analysis feature. P values were calculated using a one sample *t* test with a hypothetical mean of 1.

Liposome preparation and Rab6a labeling

Liposomes were prepared from a mixture of lipids dissolved in chloroform at (82.4% POPC, 15% POPS, 2.5% 18:1 PE MCC, 0.1% rhodamine PE (Avanti)). After mixing, they

were dried under a constant stream of argon and then desiccated in vacuum overnight. The lipid film was then resuspended with Buffer A without glycerol and passed 25X through an extruder containing a 200 nm pore size polycarbonate filter. A 3:1 ratio of Rab6a to maleimide lipid was then mixed together and incubated overnight. The next day, DTT was added to a final concentration of 10 mM to quench the reaction, and the liposomes were pelleted at 160,000g for 20 minutes to remove unlabeled Rab6a. The pellet was then washed and resuspended with Buffer A.

Single-molecule and liposome imaging

Preparation of microtubules. Microtubules were prepared as previously described (McKenney et al., 2014). Unlabeled tubulin was mixed with biotinylated tubulin and Alexa-640 labeled tubulin at a ratio of ~10:2:2 in BRB80 (80 mM PIPES, pH 6.8, 1 mM EGTA, 1 mM MgCl$_2$). 5 mM GTP was added and the mixture was incubated in a 37°C water bath for 10 min before adding. 20 M of Taxol and incubated for an additional 50 min at 37°C. Microtubules were spun over a 25% sucrose cushion at 160,000 g for 10 min in a tabletop centrifuge prior to use.

Preparation of DDB complexes and imaging. DDB complexes were formed in a 30 L reaction volume containing ~20 nM of recombinant BICD2, ~0.15 mg/ml of dynein/dynactin, and Buffer A along with 0.1 mg/ml Biotin-BSA, 0.5% pluronic acid F-127, and 0.2 mg/ml κ-casein (Buffer B). The proteins were mixed and incubate on ice for 20 min prior to use. In

experiments where Rab6a was also included, the respective construct was added to a final concentration of 1 M. Flow chambers with attached microtubules were performed as described (Schroeder and Vale, 2016). A 1:4 or 1:5 dilution of the DDB complex in Buffer B was then added in presence of 1 mM ATP and the Trolox/PCA/PCD oxygen scavenging system (Aitken et al., 2008). For processivity experiments, a SNAP-BICD2 construct labeled with the TMR-Star fluorophore from NEB was used. Because the run-lengths using Buffer B tended to span the entire lengths of our microtubules, we added 15 mM of KCl to Buffer B (termed Buffer C) for measurement of processivity. The increased amount of salt in Buffer C reduced the run length for DDB (~4 m) so that it could be measured more accurately on microtubules (average length of ~16 m used in these measurements).

For liposome assays, the same components as in the DDB mixture above was mixed in a tube, along with either Rab6a^{GTP} or Rab6a^{GDP} liposomes. The liposomes were diluted to a final concentration of ~2.5 M total lipid. After incubation, the solution was flowed in undiluted into an imaging chamber after addition of 1 mM ATP and Trolox/PCA/PCD. The amount of BICD2-GFP fluorescence on the liposomes was used to determine the average number of molecules bound to each liposome by comparing it to that of single GFP molecules captured via biotin-anti-GFP stuck onto a coverslip coated with streptavidin. Fluorescent intensities were measured by integrating the average fluorescence intensity over 5 frames at 200ms exposure and quantified with the FiJI

plugin Spot Intensity Analysis (http://imagej.net/Spot_Intensity_Analysis). Liposome GFP fluorescence (bound to glass) was normalized to single GFP fluorescent yielded an average of 6.01 BICD2 molecules per Rab6a^{GTP} liposomes (n = 6000 intensity measurements of single GFP and n = 728 intensity measurement of BICD2-GFP on liposomes).

Total internal reflection fluorescence images were acquired on a Nikon Eclipse TE200-E microscope equipped with an Andor iXon EM CCD camera, a 100x 1.49 NA objective, and MicroManager software (Edelstein et al., 2010). Exposures of 100 or 200 ms with a frame interval of 1 per sec for 300 sec was typically utilized for the acquisition. All assays were performed at room temperature.

Peroxisome Assay in U2OS cells

U2OS cells from ATCC were cultured in DMEM medium containing 10% FCS and 1x penicillin/streptomycin/glutamine. Cells were seeded in glass-bottom 96 well plates and were at ~40% confluence on the day of transfection. Cells were transfected with TransIT Lt1 as per the manufacturer's protocol with a combination of the PEX-eGFP-FRB, mCherry-BICD2-FKBP, and PEX-Rab6a plasmids and incubated overnight. The next day, 1 M of rapamycin or DMSO were added to cells and allowed to incubate at 37°C for 1 hr. 10 min before the end of this incubation, Cell Mask Far Red (Thermofisher) was added (0.5x of the manufacturer's solution) to stain the plasma membrane. Cells were then

washed with PBS and fixed with 4% paraformaldehyde (PFA) at room temperature followed by extensive washing with PBS. Cells were imaged at room temperature using an inverted Nikon Eclipse Ti microscope using a 0.75 NA 40x air objective, Andor Xyla camera, and Micro-Manager software (Edelstein et al., 2010).

Primary hippocampal neuron cultures and transfection

Primary hippocampal neuron cultures were prepared from tissue from embryonic day 18 (E18) rat brains which were shipped over-night on ice from Brainbits LLC. Cells were prepared according to provider's instructions. Briefly, the tissue was incubated with a 2 mg/ml solution of papain in Hibernate E without calcium (Braintbits) for 10 min at 30°C. The tissue was then triturated using a fire polished Pasteur pipette for 1 min and then large tissue pieces were allowed to settle for 1 min. The supernatant was collected and centrifuged at 200xg for 1 min to collect cells. After removal of most of the supernatant, the pellet was resuspended with 1 ml of NbActiv1 and the cells were counted after staining with Trypan Blue (1:5 dilution). ~50,000 cells were seeded onto poly-d lysine/laminin coated round coverslips (Corning BioCoat) placed into wells of a 24-well plate.

One day after plating, neurons were transfected using Lipofectamine 2000 (Invitrogen). Each transfection reaction contained 1 µg of total plasmid DNA along with 4 µL of

Lipofectamine reagent incubated together for 20 min at r.t. Media from the neurons was then removed and saved and fresh NbActiv was added to the wells along with the transfection mixture. After 2.5 hr at 37°C in 5% CO_2, the neurons were washed with NbActiv and the original conditioned media was added back. Cells were fixed 3 days after transfection using 4% PFA for 20 min at room temperature. After washing, the coverslips were mounted onto slides using Vectashield (Vector Labs). Neurons were imaged for both soluble GFP and mCherry-BICD2 signal at room temperature using a Zeiss Axiovert 200M microscope with a 0.5 NA 20x air objective, Hamamatsu C4742-98 CCD camera, and Micro-manager software (Edelstein et al., 2010).

Image Analysis and Quantification

Analysis of DDB and liposome motility and run length. Kymographs were created from the single molecule or liposome movies using ImageJ. The number of runs per micron of MT per unit of time was obtained from these kymographs, with each run being scored if it was >1 μm in length. P-values were calculated using an unpaired *t* test. The cumulative frequency was used for analysis of run lengths, as previously described (McKenney et al., 2014). The 1-cumulative frequency distribution was fitted with a one-phase exponential decay for run lengths of greater than 1uM, as runs shorter than this were undersampled or difficult to measure given our imaging conditions (Thorn et al., 2000).

Analysis of peroxisome clustering. The images acquired from fixed U2OS cells were processed and analyzed using the Compaction Profiler plugin previously developed for the ICY software (Mounier et al., 2012). Briefly, the fluorescent signal from the GFP channel corresponding to peroxisomes were detected after masking the shape of cell via the CellMask channel and quantified using the Spot Detector plugin in ICY. The detected fluorescence data was then passed along to the Compaction Profiler plugin, which then calculated the area of an ROI inside the cell that represents 90% of the total fluorescence signal. A higher degree of clustering results in a smaller calculated area, whereas a more diffusive signal yields a larger area. P-values were calculated using an unpaired *t* test.

Analysis of primary hippocampal neurons. Neurite lengths were measured using the soluble GFP signal from the transfected plasmid. Acquired images were processed via ImageJ. The background was subtracted using the default setting, followed by a median filter with a value of 2.0. The images were adjusted for brightness and contrast and the ImageJ plugin NeuronJ was then utilized to trace all neurites including branches from individual neurite. The longest neurite from a cell was also identified and measured. P-values were calculated using an unpaired *t* test.

Acknowledgements

References

Aitken, C.E., R.A. Marshall, and J.D. Puglisi. 2008. An oxygen scavenging system for improvement of dye stability in single-molecule fluorescence experiments. *Biophys. J.* 94:1826–1835. doi:10.1529/biophysj.107.117689.

Allan, V.J. 2011. Cytoplasmic dynein. *Biochem. Soc. Trans.* 39:1169–78. doi:10.1042/BST0391169.

Burkhardt, J.K., C.J. Echeverri, T. Nilsson, and R.B. Vallee. 1997. Overexpression of the dynamitin (p50) subunit of the dynactin complex disrupts dynein-dependent maintenance of membrane organelle distribution. *J. Cell Biol.* 139:469–484. doi:10.1083/jcb.139.2.469.

Carter, A.P., C. Cho, L. Jin, and R.D. Vale. 2011. Crystal structure of the dynein motor domain. *Science*. 331:1159–65. doi:10.1126/science.1202393.

de Chaumont, F., S. Dallongeville, N. Chenouard, N. Hervé, S. Pop, T. Provoost, V. Meas-Yedid, P. Pankajakshan, T. Lecomte, Y. Le Montagner, T. Lagache, A. Dufour, and J.-C. Olivo-Marin. 2012. Icy: an open bioimage informatics platform for extended reproducible research. *Nat. Methods*. 9:690–696. doi:10.1038/nmeth.2075.

Chen, X.J., H. Xu, H.M. Cooper, and Y. Liu. 2014. Cytoplasmic dynein: A key player in neurodegenerative and neurodevelopmental diseases. *Sci. China Life Sci.* 57:372–377. doi:10.1007/s11427-014-4639-9.

Cianfrocco, M.A., M.E. Desantis, A.E. Leschziner, and S.L. Reck-peterson. 2015. Mechanism and Regulation of Cytoplasmic Dynein. 1–26. doi:10.1146/annurev-cellbio-100814-125438.

Deng, W., C. Garrett, B. Dombert, V. Soura, G. Banks, E.M.C. Fisher, M.P. Van Der Brug, and M. Hafezparast. 2010. Neurodegenerative mutation in cytoplasmic dynein alters its organization and dynein-dynactin and dynein-kinesin interactions. *J. Biol. Chem.* 285:39922–39934. doi:10.1074/jbc.M110.178087.

Dimitriadi, M., A. Derdowski, G. Kalloo, M.S. Maginnis, B. Bliska, A. Sorkaç, K.C. Q Nguyen, S.J. Cook, G. Poulogiannis, W.J. Atwood, D.H. Hall, A.C. Hart, and E.H. by Robert Horvitz. 2016. Decreased function of survival motor neuron protein impairs endocytic pathways. doi:10.1073/pnas.1600015113.

Edelstein, A., N. Amodaj, K. Hoover, R. Vale, and N. Stuurman. 2010. Computer control of microscopes using manager. *Curr. Protoc. Mol. Biol.* 1–17. doi:10.1002/0471142727.mb1420s92.

Gama, J.B., C. Pereira, P.A. Simões, R. Celestino, R.M. Reis, D.J. Barbosa, H.R. Pires, C. Carvalho, J. Amorim, A.X. Carvalho, D.K. Cheerambathur, and R. Gassmann. 2017. Molecular mechanism of dynein recruitment to kinetochores by the Rod–Zw10–Zwilch complex and Spindly. *J. Cell Biol.* 216:943–960. doi:10.1083/jcb.201610108.

Grigoriev, I., D. Splinter, N. Keijzer, P.S. Wulf, J. Demmers, T. Ohtsuka, M. Modesti, I. V Maly, F. Grosveld, C.C. Hoogenraad, and A. Akhmanova. 2007. Rab6 regulates transport and targeting of exocytotic carriers. *Dev. Cell*. 13:305–14. doi:10.1016/j.devcel.2007.06.010.

Hafezparast, M., R. Klocke, C. Ruhrberg, A. Marquardt, A. Ahmad-Annuar, S. Bowen, G. Lalli, A.S. Witherden, H. Hummerich, S. Nicholson, P.J. Morgan, R. Oozageer, J. V Priestley, S. Averill, V.R. King, S. Ball, J. Peters, T. Toda, A. Yamamoto, Y. Hiraoka, M. Augustin, D. Korthaus, S. Wattler, P. Wabnitz, C. Dickneite, S. Lampel, F. Boehme, G. Peraus, A. Popp, M. Rudelius, J. Schlegel, H. Fuchs, M. Hrabe de Angelis, G. Schiavo, D.T. Shima, A.P. Russ, G. Stumm, J.E. Martin, and E.M.C. Fisher. 2003. Mutations in dynein link motor neuron degeneration to defects in retrograde transport. *Science*. 300:808–12. doi:10.1126/science.1083129.

Harada, A., Y. Takei, Y. Kanai, Y. Tanaka, S. Nonaka, and N. Hirokawa. 1998. Golgi vesiculation and lysosome dispersion in cells lacking cytoplasmic dynein. *J. Cell Biol.* 141:51–59. doi:10.1083/jcb.141.1.51.

Hoang, H.T., M.A. Schlager, A.P. Carter, and S.L. Bullock. 2017. DYNC1H1 mutations associated with neurological diseases compromise processivity of dynein-dynactin-cargo adaptor complexes. *Proc. Natl. Acad. Sci.* 114:1–19. doi:10.1073/pnas.1620141114.

Hoogenraad, C.C., P. Wulf, N. Schiefermeier, T. Stepanova, N. Galjart, J.V. Small, F. Grosveld, C.I. de Zeeuw, and A. Akhmanova. 2003. Bicaudal D induces selective dynein-mediated microtubule minus end-directed transport. *EMBO J.* 22:6004–15. doi:10.1093/emboj/cdg592.

Jaarsma, D., R. van den Berg, P.S. Wulf, S. van Erp, N. Keijzer, M. a Schlager, E. de Graaff, C.I. De Zeeuw, R.J. Pasterkamp, A. Akhmanova, and C.C. Hoogenraad. 2014. A role for Bicaudal-D2 in radial cerebellar granule cell migration. *Nat. Commun.* 5:3411. doi:10.1038/ncomms4411.

Kapitein, L.C., M.A. Schlager, W.A. Van Der Zwan, P.S. Wulf, N. Keijzer, and C.C. Hoogenraad. 2010. Probing intracellular motor protein activity using an inducible cargo trafficking assay. *Biophys. J.* 99:2143–2152. doi:10.1016/j.bpj.2010.07.055.

Liu, Y., H.K. Salter, A.N. Holding, C.M. Johnson, E. Stephens, P.J. Lukavsky, J. Walshaw, and S.L. Bullock. 2013. Bicaudal-D uses a parallel, homodimeric coiled

coil with heterotypic registry to coordinate recruitment of cargos to dynein. *Genes Dev.* 27:1233–46. doi:10.1101/gad.212381.112.

Martinez-Carrera, L.A., and B. Wirth. 2015. Dominant spinal muscular atrophy is caused by mutations in BICD2, an important golgin protein. *Front. Neurosci.* 9. doi:10.3389/fnins.2015.00401.

Matanis, T., A. Akhmanova, P. Wulf, E. Del Nery, T. Weide, T. Stepanova, N. Galjart, F. Grosveld, B. Goud, C.I. De Zeeuw, A. Barnekow, and C.C. Hoogenraad. 2002. Bicaudal-D regulates COPI-independent Golgi-ER transport by recruiting the dynein-dynactin motor complex. *Nat. Cell Biol.* 4:986–92. doi:10.1038/ncb891.

McKenney, R.J., W. Huynh, M.E. Tanenbaum, G. Bhabha, and R.D. Vale. 2014. Activation of cytoplasmic dynein motility by dynactin-cargo adapter complexes. *Science (80-.).* 345:337–341. doi:10.1126/science.1254198.

Mohler, J., and E.F. Wieschaus. 1986. Dominant maternal-effect mutations of Drosophila melanogaster causing the production of double-abdomen embryos. *Genetics*. 112:803–822.

Mounier, J., G. Boncompain, L. Senerovic, T. Lagache, F. Chrétien, F. Perez, M. Kolbe, J.C. Olivo-Marin, P.J. Sansonetti, and N. Sauvonnet. 2012. Shigella effector IpaB-induced cholesterol relocation disrupts the golgi complex and recycling network to inhibit host cell secretion. *Cell Host Microbe*. 12:381–389. doi:10.1016/j.chom.2012.07.010.

Neveling, K., L. a Martinez-Carrera, I. Hölker, A. Heister, A. Verrips, S.M. Hosseini-Barkooie, C. Gilissen, S. Vermeer, M. Pennings, R. Meijer, M. te Riele, C.J.M. Frijns, O. Suchowersky, L. MacLaren, S. Rudnik-Schöneborn, R.J. Sinke, K. Zerres, R.B. Lowry, H.H. Lemmink, L. Garbes, J. a Veltman, H.J. Schelhaas, H. Scheffer, and B. Wirth. 2013. Mutations in BICD2, which encodes a golgin and important motor adaptor, cause congenital autosomal-dominant spinal muscular atrophy. *Am. J. Hum. Genet.* 92:946–54. doi:10.1016/j.ajhg.2013.04.011.

Oates, E.C., A.M. Rossor, M. Hafezparast, M. Gonzalez, F. Speziani, D.G. MacArthur, M. Lek, E. Cottenie, M. Scoto, a R. Foley, M. Hurles, H. Houlden, L. Greensmith, M. Auer-Grumbach, T.R. Pieber, T.M. Strom, R. Schule, D.N. Herrmann, J.E. Sowden, G. Acsadi, M.P. Menezes, N.F. Clarke, S. Züchner, F. Muntoni, K.N. North, and M.M. Reilly. 2013. Mutations in BICD2 cause dominant congenital spinal muscular atrophy and hereditary spastic paraplegia. *Am. J. Hum. Genet.* 92:965–73. doi:10.1016/j.ajhg.2013.04.018.

Ori-McKenney, K.M., J. Xu, S.P. Gross, and R.B. Vallee. 2010. A cytoplasmic dynein tail mutation impairs motor processivity. *Nat. Cell Biol.* 12:1228–1234.

doi:10.1038/ncb2127.

Paschal, B.M., H.S. Shpetner, and R.B. Vallee. 1987. MAP 1C is a microtubule-activated ATPase which translocates microtubules in vitro and has dynein-like properties. *J. Cell Biol.* 105:1273–1282. doi:10.1083/jcb.105.3.1273.

Peeters, K., S. Bervoets, T. Chamova, I. Litvinenko, E. De Vriendt, S. Bichev, D. Kancheva, V. Mitev, M. Kennerson, V. Timmerman, P. De Jonghe, I. Tournev, J. Macmillan, and A. Jordanova. 2015. Novel mutations in the DYNC1H1 tail domain refine the genetic and clinical spectrum of dyneinopathies. *Hum. Mutat.* 36:287–291. doi:10.1002/humu.22744.

Peeters, K., I. Litvinenko, B. Asselbergh, L. Almeida-Souza, T. Chamova, T. Geuens, E. Ydens, M. Zimoń, J. Irobi, E. De Vriendt, V. De Winter, T. Ooms, V. Timmerman, I. Tournev, and A. Jordanova. 2013. Molecular Defects in the Motor Adaptor BICD2 Cause Proximal Spinal Muscular Atrophy with Autosomal-Dominant Inheritance. *Am. J. Hum. Genet.* 92:955–964. doi:10.1016/j.ajhg.2013.04.013.

Reck-Peterson, S.L., A. Yildiz, A.P. Carter, A. Gennerich, N. Zhang, and R.D. Vale. 2006. Single-Molecule Analysis of Dynein Processivity and Stepping Behavior. *Cell.* 126:335–348. doi:10.1016/j.cell.2006.05.046.

Redwine, W.B., and S.L. Reck-Peterson. 2017. The Human Cytoplasmic Dynein INteractome Reveals Novel Activators of Motility. *Elife.*

Rossor, A.M., E.C. Oates, H.K. Salter, Y. Liu, S.M. Murphy, R. Schule, M. a Gonzalez, M. Scoto, R. Phadke, C. a Sewry, H. Houlden, A. Jordanova, I. Tournev, T. Chamova, I. Litvinenko, S. Zuchner, D.N. Herrmann, J. Blake, J.E. Sowden, G. Acsadi, M.L. Rodriguez, M.P. Menezes, N.F. Clarke, M. Auer Grumbach, S.L. Bullock, F. Muntoni, M.M. Reilly, and K.N. North. 2014. Phenotypic and molecular insights into spinal muscular atrophy due to mutations in BICD2. *Brain.* doi:10.1093/brain/awu356.

Schlager, M.A., H.T. Hoang, L. Urnavicius, S.L. Bullock, and A.P. Carter. 2014a. In vitro reconstitution of a highly processive recombinant human dynein complex. *EMBO J.* 33:1855–68. doi:10.15252/embj.201488792.

Schlager, M.A., H.T. Hoang, L. Urnavicius, S.L. Bullock, and A.P. Carter. 2014b. In vitro reconstitution of a highly processive recombinant human dynein complex. *EMBO J.* 33:1855–68. doi:10.15252/embj.201488792.

Schlager, M.A., A. Serra-Marques, I. Grigoriev, L.F. Gumy, M. Esteves da Silva, P.S. Wulf, A. Akhmanova, and C.C. Hoogenraad. 2014c. Bicaudal D Family Adaptor Proteins Control the Velocity of Dynein-Based Movements. *Cell Rep.* 1–9.

doi:10.1016/j.celrep.2014.07.052.

Schlager, M. a, L.C. Kapitein, I. Grigoriev, G.M. Burzynski, P.S. Wulf, N. Keijzer, E. de Graaff, M. Fukuda, I.T. Shepherd, A. Akhmanova, and C.C. Hoogenraad. 2010. Pericentrosomal targeting of Rab6 secretory vesicles by Bicaudal-D-related protein 1 (BICDR-1) regulates neuritogenesis. *EMBO J.* 29:1637–51. doi:10.1038/emboj.2010.51.

Schroeder, C.M., and R.D. Vale. 2016. Assembly and activation of dynein-dynactin by the cargo adaptor protein Hook3. *J. Cell Biol.* 214:309–318. doi:10.1083/jcb.201604002.

Splinter, D., D.S. Razafsky, M. a Schlager, A. Serra-Marques, I. Grigoriev, J. Demmers, N. Keijzer, K. Jiang, I. Poser, A. a Hyman, C.C. Hoogenraad, S.J. King, and A. Akhmanova. 2012a. BICD2, dynactin, and LIS1 cooperate in regulating dynein recruitment to cellular structures. *Mol. Biol. Cell*. 23:4226–41. doi:10.1091/mbc.E12-03-0210.

Splinter, D., D.S. Razafsky, M. a Schlager, A. Serra-Marques, I. Grigoriev, J. Demmers, N. Keijzer, K. Jiang, I. Poser, A. a Hyman, C.C. Hoogenraad, S.J. King, and A. Akhmanova. 2012b. BICD2, dynactin, and LIS1 cooperate in regulating dynein recruitment to cellular structures. *Mol. Biol. Cell*. 23:4226–41. doi:10.1091/mbc.E12-03-0210.

Teuling, E., V. van Dis, P.S. Wulf, E.D. Haasdijk, A. Akhmanova, C.C. Hoogenraad, and D. Jaarsma. 2008. A novel mouse model with impaired dynein/dynactin function develops amyotrophic lateral sclerosis (ALS)-like features in motor neurons and improves lifespan in SOD1-ALS mice. *Hum. Mol. Genet.* 17:2849–2862. doi:10.1093/hmg/ddn182.

Thorn, K.S., J.A. Ubersax, and R.D. Vale. 2000. Engineering the processive run length of the kinesin motor. *J. Cell Biol.* 151:1093–1100. doi:10.1083/jcb.151.5.1093.

Unger, A., G. Dekomien, A. Güttsches, R. Kley, M. Tegenthoff, A. Ferbert, J. Weis, W.A. Linke, L. Martinez-carrera, and M. Storbeck. 2016. Expanding the phenotype of BICD2 mutations toward skeletal muscle involvement. 1–10.

Utskarpen, A., H.H. Slagsvold, T.-G. Iversen, S. Walchli, and K. Sandvig. 2006. Transport of ricin from endosomes to the golgi apparatus is regulated by Rab6A and Rab6A??? *Traffic*. 7:663–672. doi:10.1111/j.1600-0854.2006.00418.x.

Wharton, R.P., and G. Struhl. 1989. Structure of the Drosophila BicaudalD protein and its role in localizing the posterior determinant nanos. *Cell*. 59:881–892. doi:10.1016/0092-8674(89)90611-9.

Chapter III

Final Thoughts

Final Thoughts

Unlike in yeast, where dynein appears to only be important for mitotic spindle positioning, cytoplasmic dynein is critical in organisms ranging from flies to mammals. We know that it is involved in many aspects of both neuronal development and maintenance. Among some of these functions are: retrograde signaling via the transport of neurotrophic factors, localization of mRNA and RNP granules, neuronal migration, and protein recycling (reviewed in Levy & Holzbaur, 2006). It is easy to see, then, that modifying dynein's activity in any way could dramatically affect neuronal homeostasis. Inhibition of cytoplasmic dynein via the overexpression of the dynactin p50 subunit has been shown to abrogate retrograde transport, leading to the accumulation of aggregates at the synapse. As I have described in my dissertation, while a single point mutation in BICD2 might only slightly increase the formation of the dynein ternary complex, it is sufficient to cause a 40% reduction in the neurite growth. In addition to future experiments to generate a better understanding how this leads to diseases such as dominant spinal muscular atrophy, it is also worthwhile to first discuss adaptors as a whole.

One important question in this field is whether adaptors share a conserved mechanism for facilitating dynein complex formation. All the adaptors that have been identified thus far have shared a common feature in that they contain at least one coiled-coil domain. While structural work has given us insight into how the N-terminal coiled-

coil region of BICD2 stabilizes the tail domain of dynein and the Arp1 filament of dynactin, it is still not clear whether the coiled-coil regions of other adaptors are also involved in this interaction (Urnavicius et al., 2015).

Obtaining high resolution structures of other dynein-dynactin-adaptor complexes would be ideal, and might also provide hints as to what truly defines an adaptor protein. It might also be possible to approach this question from a computational angle. Of the adaptors that have been identified thus far, BICD2 and Spindly are the two that are most closely related. They both contain a conserved region located in the first coiled-coil of each protein. There also exists a second conserved stretch of six amino acids termed the Spindly motif that is present in both proteins. This motif classically defines the Spindly family of proteins and is necessary for the recruitment of dynein as mediated by Spindly to the kinetochore. Interestingly, an analysis of adaptors has revealed that almost all of them also possess this Spindly motif down-stream of a coiled-coil domain, and that it is important for binding to the pointed end complex of dynactin (Barisic et al., 2010). One strategy to identify additional adaptors could be to perform a bioinformatic analysis of proteins to isolate those that contain a Spindly motif next to a coiled-coil region of defined length, and subsequently using something like the peroxisome assay to further narrow down potential hits. The results of this would indicate, at minimum, whether there exists a larger family of adaptors that rely on this Spindly motif for function.

A related question that warrants further investigation is the regulation of adaptor proteins. Recent work in the Vale lab by Yuxiao Wang and Taylor Skokan has identified two novel adaptor proteins that contain EF-hands. The ability of these proteins to interact with dynein and dynactin is dictated by the concentration of calcium and suggests that there exist many ways in which a cell is able to regulate motor activity. In one case, binding of cognate cargo in the form of Rab6a vesicles is sufficient for relief of BICD2 auto-inhibition, while in the case of an EF-hand containing protein, a change in the calcium flux is necessary to stimulate motility. This allows for exquisite control over when and how dynein should be recruited to specific locations and cargoes within a cell. Rab11-FIP3, another adaptor that contains a calcium-binding domain, may share a similar mode of regulation. Another means of control might include post-translational modifications such as phosphorylation, as has been suggested for Spindly (Barisic et al., 2010).

The notion that BICD2 exists in an auto-inhibited form is not new. Since the identification of Drosophila BICD, there have been observations that indicated that full-length protein behaved differently than a C-terminal truncation (Hoogenraad et al., 2003; Stuurman et al., 1999). However, my work is the first to actively test this mechanism using an assay to directly interrogate its function and demonstrate that it is possible to activate motor complex formation via the binding of Rab6a^{GTP}. Intuitively, this mechanism for regulation makes sense; it prevents the adaptor from binding to dynein and dynactin in

the absence of cargo. BICD2 has also been shown to be recruited to nuclear pore complexes in G2 of the cell cycle via its interaction with RanBP2, which shares the same site of binding as Rab6a (Splinter et al., 2010). Future work examining whether RanBP2 can also alleviate auto-inhibition would be important for determining whether these two cellular functions of BICD2 are mutually exclusive.

The disruption of adaptor regulation and its association with human disease is another interesting area of research for the future. How might hyperactivation of BICD2 in neurons contribute to SMA? There are at least two separate but not necessarily mutually exclusive outcomes that might result from the expression of the mutant gene. The first is that the balance of BICD2 cargo in long processes such as the axon gets shifted towards the cell body. Rab6a vesicles, which are known to undergo bidirectional motility, would be biased towards the retrograde direction. Determining the contents of these vesicles could be one crucial step to understanding the etiology of the particular form of spinal muscular atrophy that is caused by these mutants. One possible hypothesis is that some essential axonal maintenance factor present in Rab6a vesicles is unable to be delivered at the proper amounts to the distal axon regions in the mutants. The lack of this protein might retard neuronal development, thus causing the observed phenotype of shorter axons observed in rat hippocampal neurons when the mutants are over-expressed.

The first outcome of mutant over-expression is increased retrograde activity, but only for vesicles that would bind to BICD2. Thus, the second possibility is that BICD2 mutants might lead to a decrease of dynein available for the transport of non-Rab6a cargos in the axon terminus. Furthermore, in the cell-based assay described in Chapter 2, peroxisomes containing mutant BICD2 formed a tighter cluster around the perinuclear region, presumably containing some level of dynein and dynactin also associated with it. This sequestration effect would contribute to a global decrease in available dynein as well. The initial studies examining the effect of BICD2 mutants in cells observed Golgi fragmentation, which has long been associated with a phenotype for dynein inhibition (Neveling et al., 2013). If the mutants are indeed sequestering dynein due to their increase propensity at forming the tripartite dynein complex, it would effectively be function as dynein inhibition for other cellular functions. Rab6a has also been shown to release Lis1 from idling dynein bound to microtubules (Yamada et al., 2013). It is also possible, then, that the reduction of Rab6a at the axon terminus eliminates a mode of dynein activation as well. Future work examining whether there is an increased in idling dynein at the microtubule plus ends and if there is an increased in the amount of dynein the cell body in neurons expressing BICD2 mutants would be crucial to further understanding the underlying reason for disease progression.

References

Barisic, M., Mikolcevic, P., Wandke, C., Rauch, V., Ringer, T., Hess, M., & Geley, S. (2010). Spindly / CCDC99 Is Required for Efficient Chromosome Congression and Mitotic Checkpoint Regulation ´ne, *21*, 1968–1981. http://doi.org/10.1091/mbc.E09

Hoogenraad, C. C., Wulf, P., Schiefermeier, N., Stepanova, T., Galjart, N., Small, J. V., … Akhmanova, A. (2003). Bicaudal D induces selective dynein-mediated microtubule minus end-directed transport. *The EMBO Journal*, *22*(22), 6004–15. http://doi.org/10.1093/emboj/cdg592

Levy, J. R., & Holzbaur, E. L. F. (2006). Cytoplasmic dynein/dynactin function and dysfunction in motor neurons. *International Journal of Developmental Neuroscience*, *24*(2–3), 103–111. http://doi.org/10.1016/j.ijdevneu.2005.11.013

Neveling, K., Martinez-Carrera, L. a, Hölker, I., Heister, A., Verrips, A., Hosseini-Barkooie, S. M., … Wirth, B. (2013). Mutations in BICD2, which encodes a golgin and important motor adaptor, cause congenital autosomal-dominant spinal muscular atrophy. *American Journal of Human Genetics*, *92*(6), 946–54. http://doi.org/10.1016/j.ajhg.2013.04.011

Splinter, D., Tanenbaum, M. E., Lindqvist, A., Jaarsma, D., Flotho, A., Yu, K. Lou, … Akhmanova, A. (2010). Bicaudal D2, dynein, and kinesin-1 associate with nuclear pore complexes and regulate centrosome and nuclear positioning during mitotic entry. *PLoS Biology*, *8*(4), e1000350. http://doi.org/10.1371/journal.pbio.1000350

Stuurman, N., Häner, M., Sassea, B., Hübner, W., Suterd, B., & Aebi, U. (1999). Interactions between coiled-coil proteins: Drosophila lamin Dm0 binds to the Bicaudal-D protein. *European Journal of Cell Biology*, *78*(4), 278–287. http://doi.org/10.1016/S0171-9335(99)80061-2

Urnavicius, L., Zhang, K., Diamant, A. G., Motz, C., Schlager, M. A., Yu, M., … Carter, A. P. (2015). The structure of the dynactin complex and its interaction with dynein. *Science*, *6*(7), 467–477. http://doi.org/10.7897/2230-8407.06796

Yamada, M., Kumamoto, K., Mikuni, S., Arai, Y., Kinjo, M., Nagai, T., … Hirotsune, S. (2013). Rab6a releases LIS1 from a dynein idling complex and activates dynein for retrograde movement. *Nature Communications*, *4*(May), 2033. http://doi.org/10.1038/ncomms3033

Appendix A

Identification of Dynein Adaptors

Appendix A

The identification of Bicaudal D2 as a dynein adaptor protein led to the natural question of whether other proteins existed that could also function as a mediator for ternary complex formation. In order to pursue this question, I worked with Richard McKenney to first identify potential candidates. From the literature, it became apparent that there existed many proteins similar to BICD2 that were known to be associated with dynein and were important for its functions. Because we were uncertain whether adaptors would contain a conserved motif or domain, it seemed prudent to not impose a stringent filter for this selection process; the only main requirement was that the protein contain a coiled-coil. The rationale for this was that the minimal BICD2 construct that is commonly used is predominantly comprised of coiled-coil stretches.

Hook3 serves as a good example of how candidates were chosen. Two papers were published around the time that we were searching from adaptors that implicated Hook as being important for early endosome trafficking in the fungi *A. nidulans* and *U. maydis* (Bielska et al., 2014; Zhang et al., 2014). It was shown in both papers that the N-terminus of Hook was necessary for binding to dynein, while its C-terminus targets it to early endosomes. The absence of Hook resulted in a decrease in early endosome movement, suggesting that it was important for both binding to the cargo and recruiting dynein. This description is reminiscent of BICD2, which was known to bind to Rab6a via its C-terminal

domain and interacted with dynein and dynactin via its N-terminus. A mammalian homolog of the Hook protein, Hook3, was thus chosen as a potential adaptor for the screen. Other dynein-associated proteins have been shown in the past to exhibit characteristics similar to Hook (Kotak et al., 2012; Yadav et al., 2012; van Spronsen et al., 2013; Wilson et al., 2005; Barisic et al., 2010). The final list of proteins to be tested for adaptor functionality were RILP, TRAK2, NuMa, Golgin160, Rab11-FIP3, Spindly, and Hook3.

Either full-length or truncated forms of the proteins were expressed and purified and tested using two assays: porcine brain lysate pull-down and single molecule TIRF. If the candidate is an adaptor, incubation of beads coated with the protein in brain lysate should pull-down both dynein and dynactin, as visualized by immunoblotting. (Fig. 1A, 1B). Secondary validation via microscopy was performed by first adding purified dynein and dynactin to the adaptor to allow for complex formation. This mixture was then flowed into chambers coated with microtubules and imaged with TIRF for both binding and motility after the addition of ATP.

From the screen, three novel dynein adaptors were identified: Rab11-FIP3, Spindly, and Hook3. This, however, does not completely eliminate the other proteins as potential adaptors. As mentioned above, in some cases, such as with NuMa, a truncated form of the protein was utilized in the assays, typically due to difficulty in purifying the

full-length version. It is thus possible that repeating the assays with full-length or different truncations could yield positive results.
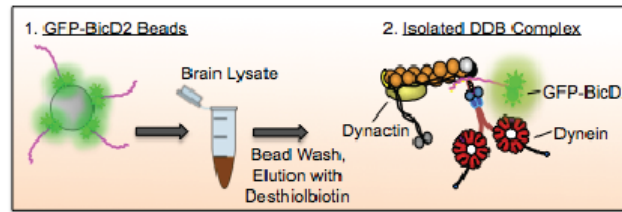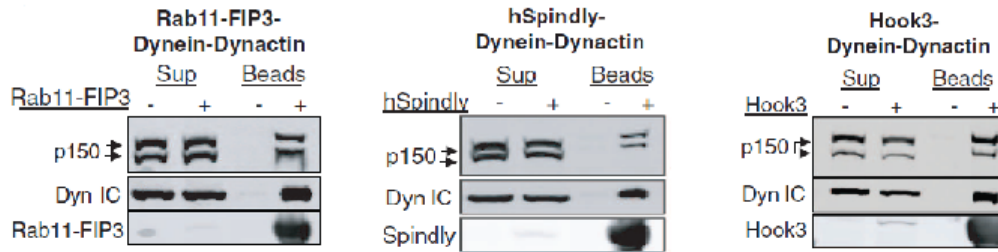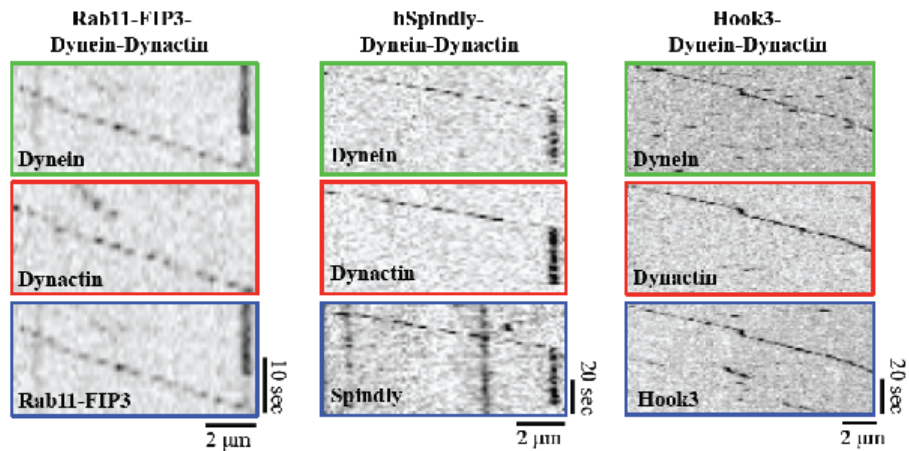
Figure 1. Assays to validate dynein adaptors

(A) Cartoon schematic of porcine brain lysate pull-down using an adaptor (BICD2) as bait on streptactin beads. (B) The pellet fraction of the pull-down from (A) for the adaptor proteins Rab11-FIP3, Spindly, and Hook3 (C) Sample kymographs of single

molecule TIRF assays using Rab11-FIP3, Spindly, and Hook3.

References

Barisic, M., P. Mikolcevic, C. Wandke, V. Rauch, T. Ringer, M. Hess, and S. Geley. 2010. Spindly / CCDC99 Is Required for Efficient Chromosome Congression and Mitotic Checkpoint Regulation ´ ne. 21:1968–1981. doi:10.1091/mbc.E09.

Bielska, E., M. Schuster, Y. Roger, A. Berepiki, D.M. Soanes, N.J. Talbot, and G. Steinberg. 2014. Hook is an adapter that coordinates kinesin-3 and dynein cargo attachment on early endosomes. *J. Cell Biol.* 204:989–1007. doi:10.1083/jcb.201309022.

Kotak, S., C. Busso, and P. Gönczy. 2012. Cortical dynein is critical for proper spindle positioning in human cells. *J. Cell Biol.* 199:97–110. doi:10.1083/jcb.201203166.

van Spronsen, M., M. Mikhaylova, J. Lipka, M. a Schlager, D.J. van den Heuvel, M. Kuijpers, P.S. Wulf, N. Keijzer, J. Demmers, L.C. Kapitein, D. Jaarsma, H.C. Gerritsen, A. Akhmanova, and C.C. Hoogenraad. 2013. TRAK/Milton motor-adaptor proteins steer mitochondrial trafficking to axons and dendrites. *Neuron.* 77:485–502. doi:10.1016/j.neuron.2012.11.027.

Wilson, G.M., A.B. Fielding, G.C. Simon, X. Yu, P.D. Andrews, R.S. Hames, A.M. Frey, A. a Peden, G.W. Gould, and R. Prekeris. 2005. The FIP3-Rab11 protein complex regulates recycling endosome targeting to the cleavage furrow during late cytokinesis. *Mol. Biol. Cell.* 16:849–860. doi:10.1091/mbc.E04-10-0927.

Yadav, S., M. a Puthenveedu, and A.D. Linstedt. 2012. Golgin160 recruits the dynein motor to position the Golgi apparatus. *Dev. Cell.* 23:153–65. doi:10.1016/j.devcel.2012.05.023.

Zhang, J., R. Qiu, H.N. Arst, M. a Peñalva, and X. Xiang. 2014. HookA is a novel dynein-early endosome linker critical for cargo movement in vivo. *J. Cell Biol.* 204:1009–26. doi:10.1083/jcb.201308009.

Publishing Agreement

It is the policy of the University to encourage the distribution of all theses, dissertations, and manuscripts. Copies of all UCSF theses, dissertations, and manuscripts will be routed to the library via the Graduate Division. The library will make all theses, dissertations, and manuscripts accessible to the public and will preserve these to the best of their abilities, in perpetuity.

Please sign the following statement:

I hereby grant permission to the Graduate Division of the University of California, San Francisco to release copies of my thesis, dissertation, or manuscript to the Campus Library to provide access and preservation, in whole or in part, in perpetuity.

_____   11/27/17
Author Signature   Date